














## RESEARCH ARTICLE

[View Article Online](#)  
[View Journal](#) | [View Issue](#)

 Cite this: *Inorg. Chem. Front.*, 2024, **11**, 7588

# Ferrocene- and ruthenium arene-containing glycomimetics as selective inhibitors of human galectin-1 and -3†

 Vojtěch Hamala, <sup>a,b</sup> Martin Kurfiřt, <sup>a,b</sup> Lucie Červenková Štátná, <sup>a</sup> Hedvika Hujerová,<sup>a</sup> Jana Bernášková, <sup>a</sup> Kamil Parkan, <sup>c,d</sup> Jakub Kaminský, <sup>d</sup> Nina Habanová, <sup>d</sup> Jaroslav Kozák, <sup>d</sup> Alžběta Magdolenová,<sup>d</sup> Martin Zavřel, <sup>d</sup> Tatiana Staroňová,<sup>e,f</sup> Veronika Ostatná, <sup>f</sup> Lucie Žaloudková,<sup>e,f</sup> Aleš Daňhel, <sup>f</sup> Jitka Holčáková,<sup>g</sup> Petr Voňka, <sup>g</sup> Roman Hrstka <sup>\*g</sup> and Jindřich Karban <sup>\*a</sup>

Galectins are a family of  $\beta$ -galactoside-binding proteins with an evolutionarily conserved carbohydrate recognition domain. Their dysregulation has been implicated in physiological and pathological processes, including fibrotic disorders, inflammation, and cancer. For example, elevated levels of galectin-1 contribute to tumor cell migration and immune evasion, whereas overexpression of galectin-3 is associated with increased invasiveness and the formation of metastasis. Pharmacological inhibition of these galectins is a promising therapeutic strategy to counteract their oncogenic effects. In this study, we synthesized a novel series of galectin inhibitors with ferrocene and ruthenium arene motifs attached to lactose, *N*-acetyllactosamine, or thiodigalactoside scaffolds. We determined their binding affinity toward human galectin-1 (*hgal*-1) and the CRD domain of human galectin-3 (*hgal*-3-CRD) using fluorescence polarization, intrinsic fluorescence of galectin tryptophan residues, and isothermal titration calorimetry. The ferrocene analogs exhibited superior affinity for both *hgal*-1 and *hgal*-3-CRD compared with ruthenium arenes. In particular, a symmetrical diferrocene thiodigalactoside complex exhibited low nanomolar affinity for *hgal*-1 and selectivity over *hgal*-3-CRD. Asymmetrical monoferrocene thiodigalactoside complexes exhibited nanomolar affinity and good selectivity for *hgal*-3-CRD. Chronopotentiometric stripping analysis demonstrated that the inhibitors stabilized *hgal*-1 against destabilization by electric field effects.  $^{19}\text{F}$  NMR experiments and molecular dynamics simulations suggested that the incorporation of the ferrocene motif limited the accessible binding modes to *hgal*-3-CRD whereas binding to *hgal*-1 remained unrestricted, resulting in attenuated binding affinities to *hgal*-3-CRD and selectivity for *hgal*-1. These results open new possibilities for the design and optimization of therapeutic organometallic galectin inhibitors.

 Received 19th June 2024,  
 Accepted 5th September 2024

DOI: 10.1039/d4qi01555j

[rsc.li/frontiers-inorganic](https://rsc.li/frontiers-inorganic)
<sup>a</sup>Institute of Chemical Process Fundamentals of the CAS, v. v. i., Rozvojová 1/135, 165 00 Praha, Czech Republic. E-mail: karban@icpf.cas.cz

<sup>b</sup>Department of Organic Chemistry, University of Chemistry and Technology, Technická 5, 166 28 Praha, Czech Republic

<sup>c</sup>Department of Chemistry of Natural Compounds, University of Chemistry and Technology, Prague, Technická 5, 166 28 Prague, Czech Republic

<sup>d</sup>Institute of Organic Chemistry and Biochemistry of the CAS, v. v. i., Flemingovo nám. 542, 160 00 Praha, Czech Republic

<sup>e</sup>Department of Biochemistry, Faculty of Science, Masaryk University, Kotlářská 2, 602 00 Brno, Czech Republic

<sup>f</sup>Institute of Biophysics of the CAS, v. v. i., Královopolská 135, 612 00 Brno, Czech Republic

<sup>g</sup>Research Centre for Applied Molecular Oncology, Masaryk Memorial Cancer Institute, Žlutý kopec 7, 656 53 Brno, Czech Republic. E-mail: hrstka@mou.cz

 †Electronic supplementary information (ESI) available. See DOI: <https://doi.org/10.1039/d4qi01555j>

## Introduction

Lectins are glycan-binding proteins that are abundant in all kingdoms of life.<sup>1</sup> In humans, binding of glycans to lectins is essential for many physiological and pathological processes including host–pathogen interactions, inflammation, auto-immune disorders, and cancer progression.<sup>2</sup> Although the key roles of lectins in pathologies and their widespread occurrence make them an important target for drug development,<sup>2b</sup> their pharmacological inhibition by small molecule inhibitors remains underexplored because of the perceived poor druggability of lectins.<sup>3</sup> Ligand binding to the shallow water-exposed binding cavity of lectins is associated with a high desolvation penalty, moderate binding affinities of monovalent sugars, and little ability of an inhibitor to form additional productive



interactions within the binding site.<sup>4</sup> Moreover, carbohydrates have poor pharmacokinetic properties,<sup>4d</sup> and because lectins form homologous families that bind the same structural motif, it is difficult to achieve selectivity in lectin inhibition. Despite these extraordinary challenges, developments in glycochemistry over the past 20 years have produced potent lectin inhibitors.<sup>4b</sup> The most successful approach in the design of lectin inhibitors relies on synthetically modified endogenous carbohydrate ligands (glycomimetics).<sup>4b</sup> Several glycomimetic lectin inhibitors have entered advanced phases of clinical trials,<sup>4b,5</sup> but with the exception of GalNAc-siRNA conjugates, none others have yet been marketed.<sup>4b</sup> Thus, the need for innovative approaches to expand the available chemical space diversity in the design of lectin inhibitors is undeniable.

Galectins are a family of animal lectins that non-covalently bind a  $\beta$ -galactopyranoside motif in membrane-bound and extracellular glycans through an evolutionarily conserved

binding site located within a carbohydrate recognition domain (CRD).<sup>4c,6</sup> Natural disaccharide galectin ligands, such as lactose (Lac) **1** and *N*-acetyllactosamine (LacNAc) **2** (Fig. 1A), bind the highly conserved region of the CRD termed subsites C and D, with each subsite accommodating one hexopyranose moiety (Fig. 1A).<sup>7</sup> The  $\beta$ -galactopyranoside moiety in these disaccharides is recognized by subsite C. Two additional monosaccharides, which can be attached to the 3'-position of the galactopyranoside moiety in endogenous ligands, are recognized by the less conserved extension of the binding groove termed subsites A and B (Fig. 1A and B).<sup>7a,b</sup> The loosely defined subsite E can interact with the substituents attached to the reducing end of the monosaccharide occupying subsite D (Fig. 1B).<sup>7d,8</sup> Galectins are implicated in several pathologies including fibrotic diseases, inflammation, and cancer.<sup>9</sup> Among sixteen mammalian galectins,<sup>7b</sup> human galectin-1 (*hgal-1*) and -3 (*hgal-3*) are probably the most studied to date due to their

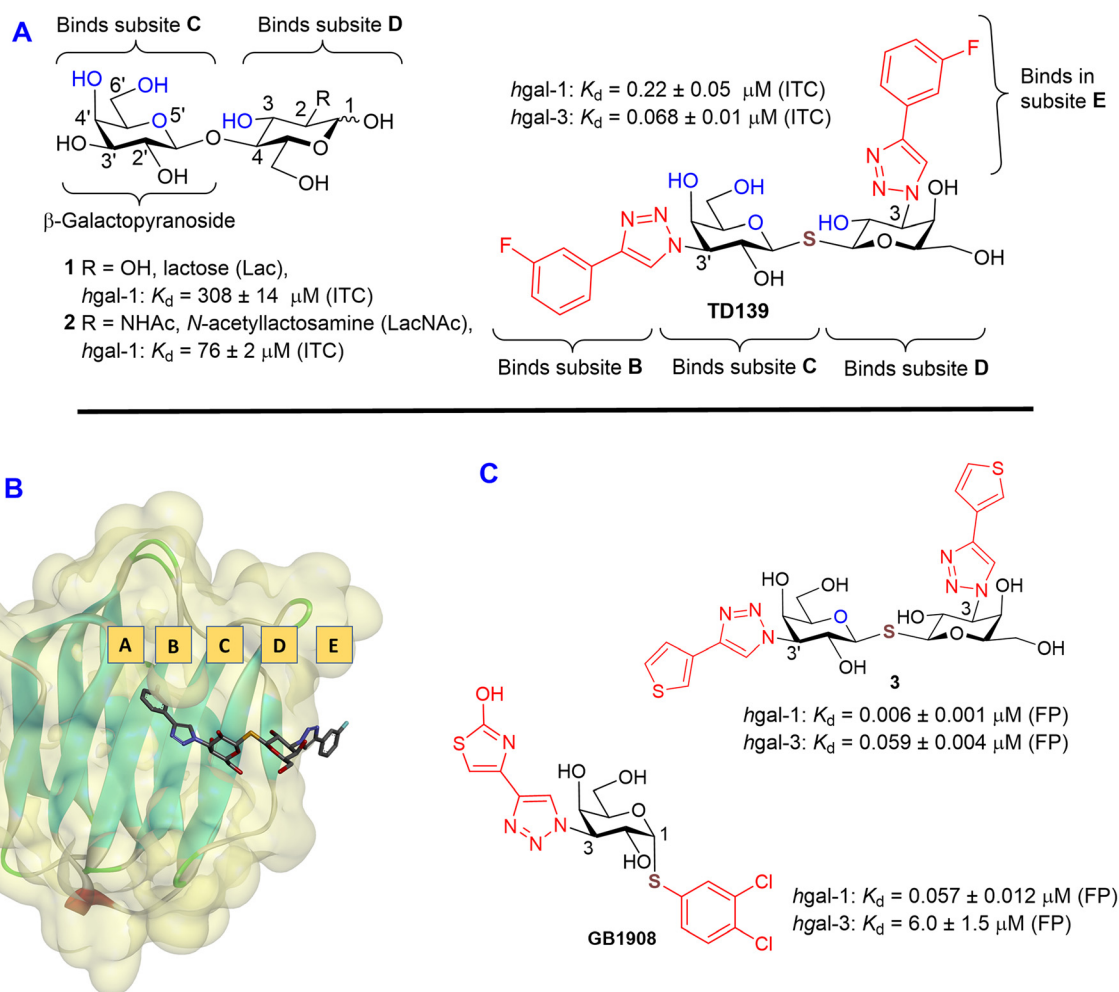


**Fig. 1** (A) Structures, numbering, and dissociation constants  $K_d$  of natural disaccharide galectin ligands **1** and **2**, and the galectin inhibitor **TD139** determined by isothermal titration calorimetry (ITC).<sup>12a</sup> Oxygen functionalities critical for binding are shown in blue, 3-fluorophenyl-triazole moiety of **TD139** is shown in red. (B) Binding subsites A–E are shown for the complex of **TD139** with *hgal-3*-CRD (PDB: 5H9P). (C) Structures of thiophene-derived *hgal-1* inhibitor **3**, thiazole-derived *hgal-1* inhibitor **GB1908** and their dissociation constants  $K_d$  determined by competitive fluorescence polarization (FP),<sup>13</sup> (hetero)aromatic moieties shown in red.



expression in many tissues and their prominent role in diseases.<sup>4c,10</sup> The involvement of galectins in pathologies is complex because galectins are multifunctional proteins whose functions depend on their cellular and tissue localization.<sup>11</sup> Moreover, different galectins can play opposite roles in disease progression.<sup>10</sup> Therefore, the availability of galectin inhibitors that are highly selective for individual galectins is essential for both fundamental research and drug development.

Typical glycomimetic small molecule galectin inhibitors comprise a galactose-containing mono- or disaccharide scaffold capable of forming the critical hydrogen bonds found in natural agonists **1** and **2** (Fig. 1A).<sup>8</sup> The scaffold is typically decorated with aromatic non-polar substituents that introduce additional interactions within the binding groove.<sup>8</sup>

The glycomimetic inhibitor **TD139** (later renamed **GB0139**, Fig. 1A) targets four subsites and illustrates this approach.<sup>14</sup> The hydroxyl groups at the 3-, 4'- and 6'-positions of natural ligands **1** and **2** (including their stereochemistry), the pyranose oxygen O5', and the hydrophobic  $\alpha$ -side of the galactoside residue are reproduced in the thiodigalactoside scaffold of **TD139**, and direct the inhibitor into subsites C and D (Fig. 1A) *via* key interactions with amino acid residues in these subsites. The fluorophenyl-triazole moiety forms guanidinium-arene cation- $\pi$  interactions with the arginine residues Arg144 and Arg186 in subsites B and E of *hgal-3*, respectively, while fluorine is involved in orthogonal multipolar interactions<sup>15</sup> with the polypeptide backbone, collectively leading to nanomolar affinities toward *hgal-3* and approximately 3-fold weaker binding to *hgal-1* according to ITC (Fig. 1A).<sup>12b</sup> Modifications of **TD139** and other inhibitors resulted in a series of excellent *hgal-3* selective disaccharide<sup>8,16</sup> and monosaccharide<sup>17</sup> inhibitors. **TD139** entered the Phase IIb of clinical trials for the treatment of idiopathic pulmonary fibrosis (IPF), but unfortunately failed due to its low efficacy and its development for IPF treatment was discontinued.<sup>18</sup>

Although the development of *hgal-3* inhibitors has advanced considerably, the development of potent *hgal-1* selective inhibitors remains challenging despite their therapeutic potential.<sup>19</sup> To the best of our knowledge, the only reported small molecule, single-digit nanomolar inhibitors of *hgal-1* are the thien-3-yl derivative **3**<sup>13a,14</sup> (Fig. 1C) and its thiazol-2-yl analog.<sup>13a</sup> Both had an approximately 10-fold selectivity for *hgal-1* over *hgal-3* as determined by a competitive fluorescence polarization (FP) assay. However, no further bioactivity of compound **3** has been reported, and it appears that this inhibitor is not being further developed. Very recently, a thiogalactoside-based inhibitor named **GB1908** with a two orders of magnitude *hgal-1* selectivity has been reported (Fig. 1C).<sup>13b</sup>

Recent X-ray diffraction and <sup>19</sup>F NMR studies have suggested differences between *hgal-1* and *hgal-3* in the binding mode of **TD139** for subsites B and E.<sup>12b</sup> Inspired by these findings, we hypothesize that lipophilic barrel-shaped organometallic complexes such as ferrocene or cyclopentadienyl-ruthenium arenes may exploit these differences and interact with the binding subsites of galectins more efficiently or selectively than the planar fluorophenyl moiety, leading to higher

binding affinity or selectivity. Organotransition metal complexes, due to their three-dimensional coordination sphere, offer structural diversity in protein-ligand interactions that is inaccessible to purely organic compounds.<sup>20</sup> For example, improved affinity or selectivity after substituting a ferrocene moiety for a planar arene has been reported for the anticancer drugs paclitaxel,<sup>21</sup> tamoxifen,<sup>20c</sup> the drug candidate plinabulin,<sup>22</sup> and the dopamine D<sub>3</sub> receptor antagonist BP 897.<sup>23</sup> In spite of their advantages, organotransition metal complexes have not been tested as antagonists in lectin inhibition, although multivalent lactose-ferrocene conjugates have been evaluated as electrochemical probes for the detection of galectin-3.<sup>24</sup>

We prepared a series of lactose, *N*-acetyllactosamine- and thiodigalactoside-based inhibitors bearing ferrocene or pentamethylcyclopentadienyl ruthenium arene complexes and determined their affinities to *hgal-1* and *hgal-3* using the FP assay, intrinsic fluorescence of galectin tryptophan residues, and ITC. Here, we report that introducing two ferrocene-triazole moieties into the thiodigalactoside scaffold resulted in an *hgal-1* inhibitor with potency comparable to **TD139** but with up to 50-fold higher selectivity for *hgal-1* over *hgal-3*, highlighting the potential of organometallic fragments in the design of lectin inhibitors. Subsequent <sup>19</sup>F{<sup>1</sup>H} NMR monitoring of the 3-fluorophenyl-triazole moiety and molecular dynamics simulations were used to explain the differences in the binding mode between *hgal-1* and *hgal-3*. In addition, the electrochemical activity of selected ferrocene derivatives was studied by cyclic voltammetry (CV), and the ability of the synthesized inhibitors to stabilize *hgal-1* against electric current was evaluated using chronopotentiometric stripping analysis.

## Results

### Synthesis of galectin antagonists

The ferrocenyl and ruthenium arene moieties were attached to the selected disaccharide scaffolds *via* a 1,2,3-triazole linker substituted at the 4-position with an organocomplex (Fig. 2C). The linker was formed by a copper(i)-catalyzed cycloaddition reaction between ferrocenyl- or phenylacetylene and an azido group at the selected positions of the disaccharides (Fig. 2, substituents **R**<sup>1</sup>, **R**<sup>2</sup>, **R**<sup>3</sup>, **R**<sup>3'</sup>). These positions were chosen because their modifications generally do not interfere with recognition by galectins and organometallic substituents at these positions enabled us to explore possible attractive interactions with subsites A/B and E flanking the most conserved region of subsites C and D.<sup>7b,8,25</sup> For Lac- and LacNAc-derived galectin ligands, we decided to attach the organometallic substituent at the reducing end anomeric position (Fig. 2A, substituent **R**<sup>1</sup>) to exploit possible interactions with subsite E. Similar reasoning applies to the 3'-OH hydroxyl of *N*-acetyllactosamine **2** (Fig. 2A, substituent **R**<sup>3'</sup>), which points toward subsites A and B. In addition, the 2-position of the lactosamine scaffold (Fig. 2A, substituent **R**<sup>2</sup>) was also modified because this position tolerates modifications with bulky sub-



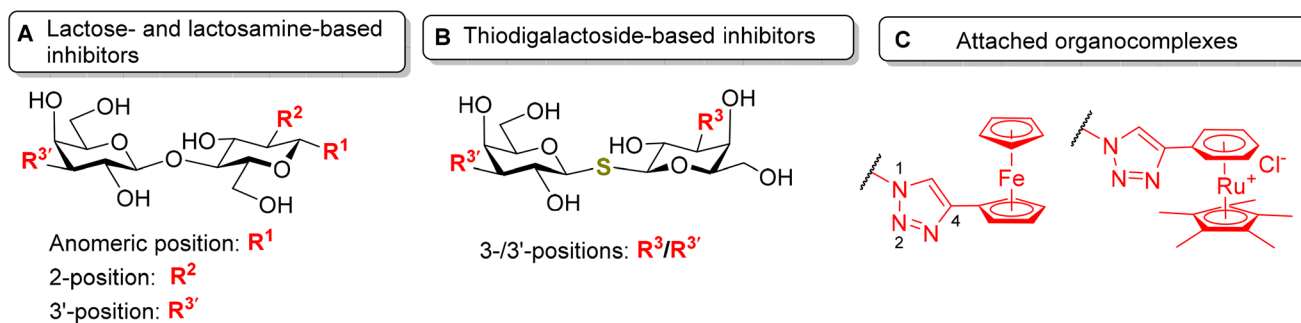


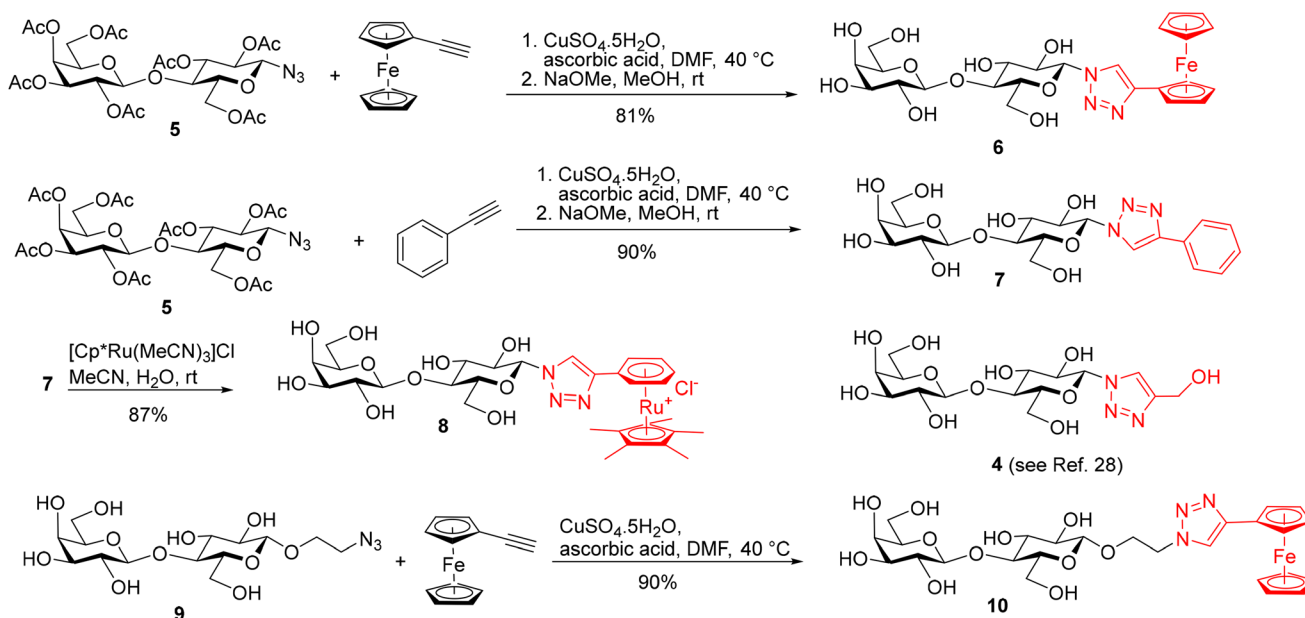
**Fig. 2** The positions selected for the attachment of modifying substituents to (A) lactose ( $R^2 = \text{OH}$ ) or lactosamine ( $R^2 = \text{NH}_2$ ), (B) thiodigalactoside, (C) Organocomplexes attached to carbohydrate scaffolds and numbering of the 1,2,3-triazole linking moiety.

stituents.<sup>7b</sup> For the symmetrical thiodigalactoside scaffold, we modified the 3/3'-position (Fig. 2B, substituents  $R^3/R^{3'}$ ). Modification at this position with an arene group has previously produced potent galectin inhibitors.<sup>8,26</sup> The ferrocene moiety was introduced directly into the disaccharide scaffold by azide-alkyne cycloaddition of the corresponding azido-disaccharides and ethynylferrocene. The (pentamethylcyclopentadienyl)ruthenium arene moiety was introduced by the complexation reaction of a phenyltriazole moiety with the  $[\text{Cp}^*\text{Ru}(\text{MeCN})_3]\text{Cl}$  complex generated *in situ*.<sup>27</sup> Non-metallic compounds bearing a hydroxymethyl, phenyl, or 3-fluorophenyl substituent attached to the disaccharide scaffold *via* a triazole linker were prepared for comparison (Scheme 1, compounds 4 and 7; Scheme 3, compounds 26, 28 and 29; Scheme 4, compound 37).

The synthesis of Lac-derived galectin ligands 4, 6–8, and 10 modified at the anomeric position is summarized in Scheme 1. Hydroxymethyl-triazole-substituted lactose 4 was

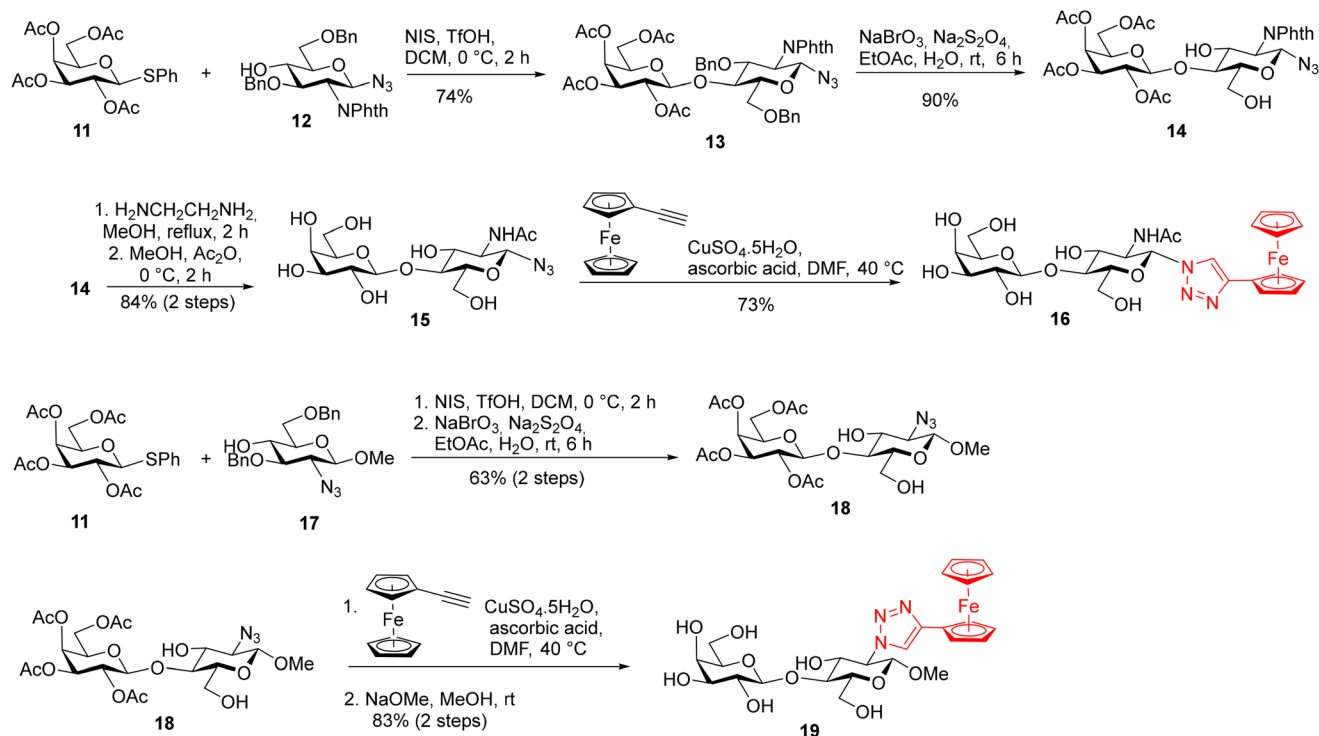
prepared for comparison as reported.<sup>28</sup> Starting azido disaccharides 5<sup>29</sup> and 9<sup>30</sup> were prepared from lactose 1 as reported and converted to the target ferrocene analogs 6 and 10 using cycloaddition with ethynylferrocene as the key reaction. The phenyl triazole 7 was obtained from azide 5 by reaction with phenyl acetylene followed by Zemplén deacetylation. Phenyl analog 7 was subjected to the complexation reaction with the  $[\text{Cp}^*\text{Ru}(\text{MeCN})_3]\text{Cl}$  complex generated *in situ* from the tetramer  $[\text{Cp}^*\text{RuCl}]_4$  as described previously.<sup>27</sup> This complexation reaction afforded the corresponding ruthenium arene 8 (Scheme 1).

The synthesis of LacNAc-derived galectin ligands 16 and 19 modified at the 1- and 2-positions, respectively, is summarized in Scheme 2. Azides 15 and 18 for the copper-catalyzed cycloaddition were prepared from monosaccharide building blocks by chemical glycosylation. *N*-Acetyllactosaminyl azide 15 was obtained by NIS/TfOH-promoted glycosylation<sup>31</sup> of known 2-phthalimido- $\beta$ -glucosyl-azide 12<sup>32</sup> with thiogalactoside 11<sup>33</sup>



**Scheme 1** Synthesis of galectin ligands 4, 6–8, and 10 derived from lactose modified at the anomeric position.





**Scheme 2** Synthesis of galectin ligands **16**, and **19** derived from LacNac modified at the 1- and 2-positions.

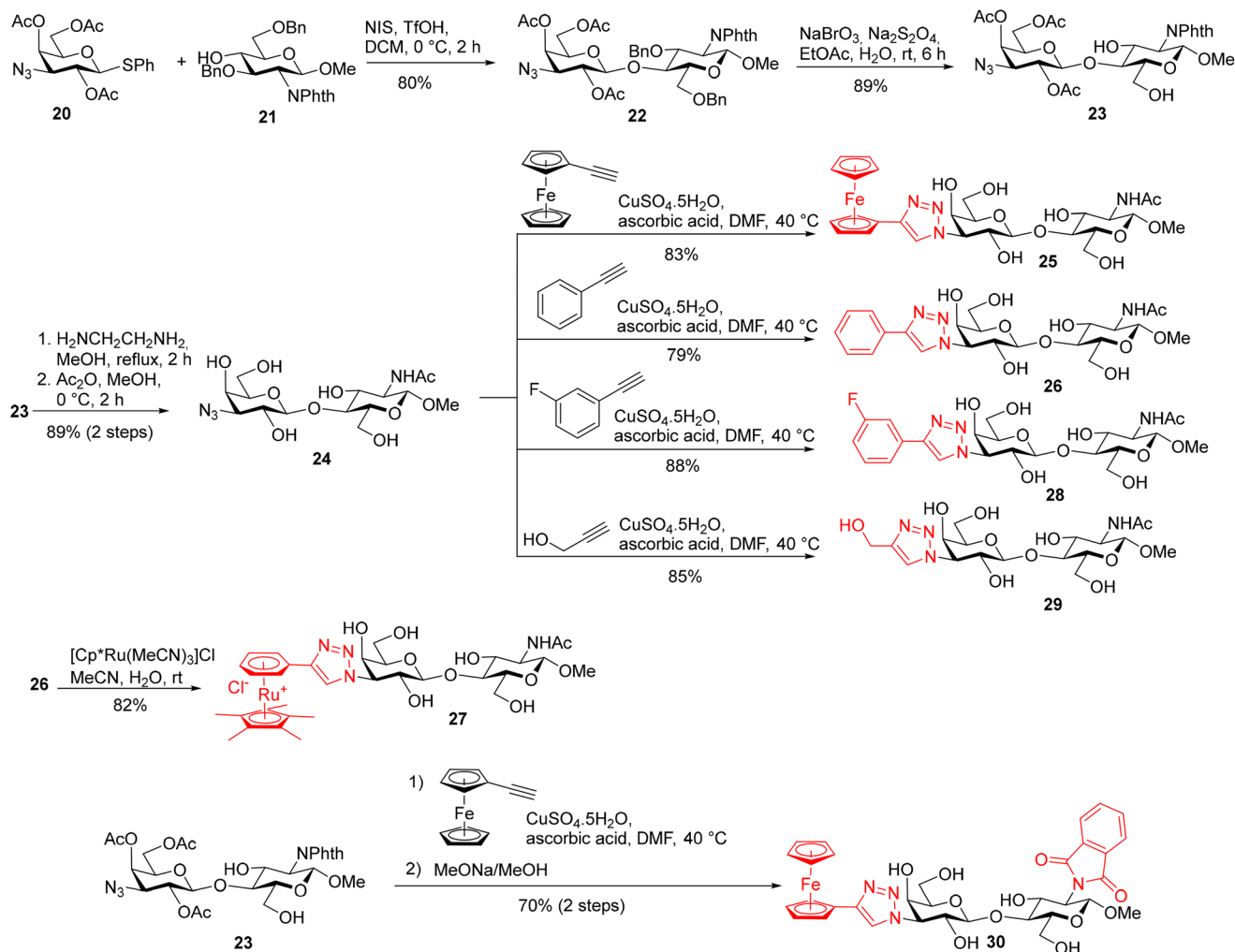
followed by sequential deprotection, using first oxidative de-*O*-benzylation with the NaBrO<sub>3</sub>/Na<sub>2</sub>S<sub>2</sub>O<sub>4</sub> system<sup>34</sup> to give compound **14**, then treatment with ethylenediamine in refluxing methanol to liberate the 2-amino group,<sup>35</sup> and finally *N*-acetylation (Ac<sub>2</sub>O, MeOH). Methyl 2-azido-lactoside **18** was obtained by NIS/TfOH-promoted glycosylation of methyl 2-azido-β-glucoside **17**<sup>36</sup> with thiogalactoside **11** followed by oxidative de-*O*-benzylation. Copper(I)-catalyzed cycloaddition between azido disaccharides **15**, and **18** and ethynylferrocene, followed by Zemplén deacetylation in the case of acetylated disaccharide **18**, afforded the target ferrocenyl-triazole-substituted disaccharides **16** and **19** (Scheme 2).

The synthesis of LacNac analogs modified at the 3'-position is described in Scheme 3. The methyl β-glycosides **23** and **24** of 3'-azido-LacNac required for azide-alkyne cycloaddition were synthesized by glycosylation of methyl 2-phthalimido-β-glucoside **21**<sup>37</sup> with 3'-azido-thiogalactoside **20**.<sup>38</sup> The resulting disaccharide **22** was oxidatively de-*O*-benzylated to yield diol **23** that was subjected to phthalimide deprotection (ethylenediamine in refluxing MeOH) and *N*-acetylation to afford the 3'-azido-LacNacβ-OME **24**. Copper(I)-catalyzed cycloaddition between azido disaccharides **23**, and **24** and ethynylferrocene, followed by Zemplén deacetylation in the case of acetylated disaccharide **23**, afforded the target ferrocenyl-triazole-substituted disaccharides **30** and **25**, respectively. The bulky phthalimido group (Phth) was retained at the 2-position of disaccharide **30** because a large aromatic substituent at this position may influence the selectivity in interactions with galectins. For comparison, 3-fluorophenyl-triazole-substituted LacNac **28**

and hydroxymethyl-triazole-substituted LacNac **29** were prepared from disaccharide **24** by cycloaddition with 3-fluorophenylacetylene and propargyl alcohol, respectively (Scheme 3). The cycloaddition of azide **24** with phenylacetylene afforded disaccharide **26** carrying a phenyl-triazole ligand suitable for the complexation reaction with the [Cp\*Ru(MeCN)<sub>3</sub>]Cl complex, which afforded the corresponding ruthenium arene **27** (Scheme 3). The parent disaccharides **26** along with disaccharide **7** (Scheme 1), both modified with the phenyl-triazole moiety, were also used as the reference compounds to determine how the substitution of the ruthenium arene or ferrocene for a planar phenyl substituent influenced the affinity. All Lac- and LacNac-based ligands were prepared as β-anomers at the reducing end anomeric position. When this anomeric position did not carry a modifying organometallic substituent, it was protected as a methyl β-glycoside (compounds **19**, **25**–**30**) to prevent the formation of a mixture of anomers.

For the thiodigalactoside-based inhibitors, we attached the modifying substituent at the 3- and 3'-positions of the thiodigalactoside scaffold (Fig. 2B), as previous work has documented that binding to galectins benefits from the attachment of arene-triazole substituents at these positions.<sup>14</sup> This produced compounds **34**, **36**–**38**, **41**, and **42** (Scheme 4). Starting 3-azido-thiodigalactoside **33** was obtained by the tetrabutylammonium fluoride-promoted reaction of 3-azido-galactosyl bromide **31**<sup>39</sup> with thiogalactoside **32**<sup>40</sup> in acetonitrile following the published protocol (Scheme 4).<sup>40,41</sup> 3,3'-Diazido-thiodigalactoside **35**,<sup>26c,39</sup> 3,4,5-trifluorophenyl-analog **39**,<sup>16</sup> and 3-fluorophenyl





**Scheme 3** Synthesis of galectin ligands **25–30** derived from LacNAc modified at the 3'-position.

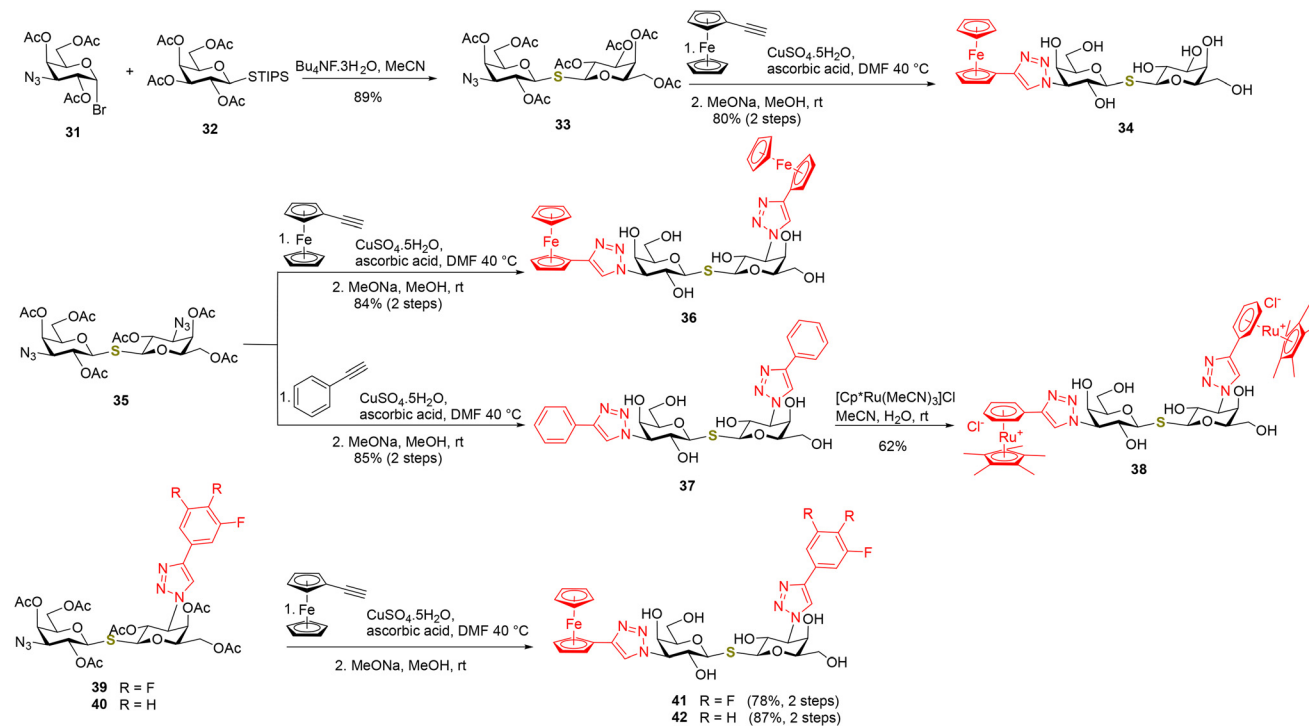
analog **40**<sup>16</sup> were prepared as reported. Cycloaddition of azides **33**, **35**, **39**, and **40** with ethynylferrocene followed by Zemplén deacetylation gave ferrocenyl-triazole-substituted analogs **34**, **36**, **41**, and **42**, respectively, whereas azide-alkyne cycloaddition of diazide **35** with phenylacetylene afforded the phenyl-triazole ligand **37** (Scheme 4). The complexation reaction of compound **37** with  $[\text{Cp}^*\text{Ru}(\text{MeCN})_3]\text{Cl}$  generated *in situ* was expected to afford the bisruthenium arene disaccharide **38**. The product produced the expected molecular ion mass in high resolution mass spectra; however, the  $^1\text{H}$  NMR spectrum showed two signals for the triazole proton and four signals for the methyl protons of the pentamethylcyclopentadienyl ring. We speculate that compound **38** was prepared as a mixture of four inseparable stereoisomers due to hindered rotation at the bond between the triazole and the phenyl ligand. All prepared ferrocenes were obtained as either crystalline or amorphous solids; most of them with limited solubility in water (see ESI for details, section B.2.†), whereas the ruthenium arenes were obtained as white amorphous solids with good water solubility. Both types of compounds exhibited stability in air and in

aqueous or DMSO solutions, as confirmed over a period of three weeks.

### Compound characterization

**NMR and HRMS spectroscopy.** The structure of the prepared compounds was confirmed by NMR and HRMS spectroscopy. The 1,2-*trans* (or  $\beta$ -) configuration of the newly formed glycosidic linkage in disaccharides **13**, **18**, **22**, and **33**, was evidenced by the magnitude of the coupling constant  $^3J_{(\text{H}-1',\text{H}-2')} = 8.0\text{--}9.8$  Hz. Ferrocenyl- or phenyltriazole-substituted disaccharides **6**, **7**, and **16**, obtained from glycosyl azides **5** and **15** by cycloaddition, retained the  $\beta$ -configuration at the 1-position and the  $^4\text{C}_1$  chair conformation of both pyranose rings, as evidenced by the values of the vicinal coupling constants  $^3J_{\text{H,H}}$  (ESI, Table S1†). The galactoside ring also retained its  $^4\text{C}_1$  chair conformation after the attachment of the modifying substituent at the 3/3'-position (compounds **25–30**, **34**, **36–38**, **41** and **42**). When signal overlap in  $^1\text{H}$  NMR spectra precluded direct determination of the diagnostic  $^3J_{\text{H,H}}$  couplings, 2D  $^1\text{H}$ - $^{13}\text{C}$  gHSQC NMR spectra were used for their estimation.





**Scheme 4** Synthesis of galectin ligands **34**, **36**–**38**, **41** and **42** derived from thiodigalactoside modified at the 3 and 3'-positions.

The formation of 1,2,3-triazole was also confirmed by NMR spectroscopy. The proton of the triazole CH group resonated at 8.01–8.90 ppm in  $^1\text{H}$  NMR spectra, while the corresponding carbon resonated at 119.8–124.7 ppm in  $^{13}\text{C}$  NMR spectra, which is characteristic of 1,4-substituted 1,2,3-triazoles.<sup>42</sup> The quaternary carbon of the 1,2,3-triazole ring showed a chemical shift in the range of 141.8–148.4 ppm. Ruthenium complexation led to shielding of the corresponding phenyl ring,<sup>27</sup> resulting in the decreased values of the proton and carbon chemical shifts ( $\delta_{\text{H}} = 5.95$ – $6.64$  ppm/ $\delta_{\text{C}} = 84.98$ – $99.3$  ppm for the phenyl ring in the ruthenium complexes,  $\delta_{\text{H}} = 7.30$ – $7.88$  ppm/ $\delta_{\text{C}} = 125.0$ – $131.9$  ppm for the phenyl rings in the parent phenyl-substituted disaccharides).

**Cyclic voltammetry.** Ferrocene is a widely used electrochemical redox probe, particularly for biological applications in conjugation with biomolecules.<sup>43</sup> In this study, we established the electrochemical activity of three inhibitors with the ferrocenyl-triazole substituent (**6**, **25**, and **36**) in comparison with ferrocenecarboxylic acid (**FcCOOH**)—a reference electrochemical redox probe—using cyclic voltammetry (CV) at a basal-plane pyrolytic graphite electrode (bPGE).<sup>44</sup> Unmodified disaccharides are electrochemically inactive substances. Because of the presence of readily oxidizable ferrocene tag(s), compounds **6**, **25**, and **36** offered reversible double peak with  $E_{1/2}$  varying between 300 mV (**25**) and 323 mV (**36**), similar to the probe **FcCOOH** with  $E_{1/2} = 320$  mV (Fig. S1 and Table S2 in the ESI†).  $\Delta E_{\text{p}} = 84$  mV of **FcCOOH** was approximately 6 mV (**6**) to 14 mV (**25**) higher than  $\Delta E_{\text{p}}$  of the corresponding ferrocenyl-triazole-modified disaccharides and approximately 25 mV

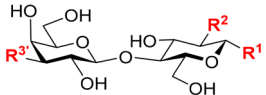
higher than the theoretical value of 59 mV for an ideally reversible system. Together with higher  $J_{\text{p}}^{\text{a}}/J_{\text{p}}^{\text{c}}$  ratios ranging from 1.67 to 2.14, with an ideal value of 1.0, it is possible to attribute the ferrocene redox signals observed at bPGE to quasi-reversible processes,<sup>45</sup> which are not significantly affected by the disaccharide structures. For more details, see ESI, pages S24–S28.†

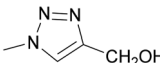
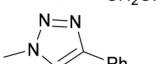
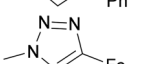
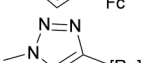
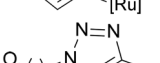
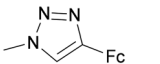
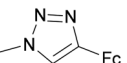
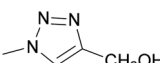
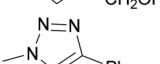
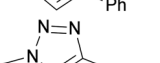
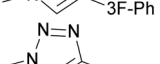
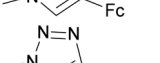
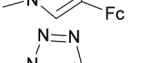
### Binding to *hgal-1* and *hgal-3*

**Competitive fluorescence polarization (anisotropy) assay.** We screened the affinity of all prepared organometallic complexes and the corresponding nonmetallic reference compounds to *hgal-1* and human galectin-3 CRD domain (*hgal-3*-CRD) using a competitive FP assay.<sup>46</sup> This assay allows a rapid determination of the apparent inhibition constant  $K_{\text{i}}$  with minimal consumption of the inhibitor (Tables 1 and 2, see the ESI† for the details of the calculation).<sup>46</sup> The *hgal-3*-CRD was employed instead of *hgal-3* to facilitate comparison with the literature data and the ITC measurements (*vide infra*).<sup>47</sup> We prepared and used methyl  $\beta$ -glycoside of LacNAc, designated 2 $\beta$ -OMe in his study, as the parent compound for the comparison with the LacNAc-derived ligands in FP and ITC assays.<sup>36</sup>

The attachment of an organometallic moiety to positions 1 and 2 of disaccharides Lac and LacNAc was aimed at the formation of additional interactions with the galectin subsite E.<sup>48</sup> Both galectins contain an arginine residue in this subsite (Arg74 in *hgal-1* and Arg186 in *hgal-3*) capable of forming cation- $\pi$  interactions with arene moieties of the inhibitor.<sup>7d,49</sup> On the whole, modifications at these positions mostly resulted in a modest improvement in binding affinity (Table 1, entries



**Table 1** Apparent inhibition constant  $K_i$ , relative potency  $rp^a$  and selectivity values obtained from competitive fluorescence polarization for inhibitors derived from Lac and LacNAc


Entry	R <sup>1</sup>	R <sup>2</sup>	R <sup>3</sup>	Compound	$K_i$ ( <i>hgal</i> -1) ( $\mu$ M)	$rp$ ( <i>hgal</i> -1)	$K_i$ ( <i>hgal</i> -3-CRD) ( $\mu$ M)	$rp$ ( <i>hgal</i> -3-CRD)	Selectivity to <i>hgal</i> -1 <sup>b</sup>
Lac-derived inhibitors <sup>c</sup>									
1	OH	OH	OH	<b>1</b> (lactose)	334 ± 28	1.0	94 ± 7	1.0	0.28
2		OH	OH	<b>4</b>	157 ± 31	2.1	55 ± 4	1.7	0.35
3		OH	OH	<b>7</b>	241 ± 36	1.4	67 ± 7	1.4	0.28
4		OH	OH	<b>6</b>	105 ± 20	3.2	35 ± 1	2.7	0.33
5		OH	OH	<b>8</b>	262 ± 51	1.3	132 ± 15	0.7	0.50
6		OH	OH	<b>10</b>	141 ± 6	2.4	30 ± 1	3.1	0.21
LacNAc-derived inhibitors <sup>c</sup>									
7	OMe	NHAc	OH	<b>2</b> $\beta$ -OMe <sup>d</sup>	182 ± 12	1.0	49 ± 3	1.0	0.27
8		NHAc	OH	<b>16</b>	73 ± 19	2.5	15 ± 1	3.3	0.20
9	OMe		OH	<b>19</b>	54 ± 2	3.4	3.9 ± 0.1	13	0.07
10	OMe	NHAc		<b>29</b>	43 ± 8	4.2	22 ± 5	2.2	0.51
11	OMe	NHAc		<b>26</b>	5.2 ± 0.8	35	2.7 ± 0.7	18.1	0.52
12	OMe	NHAc		<b>28</b>	1.7 ± 0.1	107	0.26 ± 0.01	188	0.15
13	OMe	NHAc		<b>25</b>	3.7 ± 1.2	49	5.0 ± 0.2	10	1.35
14	OMe	NPhth		<b>30</b>	3.4 ± 0.5	54	1.3 ± 0.1	38	0.38
15	OMe	NHAc		<b>27</b>	78 ± 11	2.3	14.8 ± 3.9	3.3	0.19

<sup>a</sup> Relative potency defined as  $rp = K_i(\text{Lac } \mathbf{1})/K_i(\text{inhibitor})$  for Lac-derived inhibitors,  $rp = K_i(2\beta\text{-OMe})/K_i(\text{inhibitor})$  for LacNAc-based inhibitors.  
<sup>b</sup> Defined as the ratio  $K_i(\text{hgal-3-CRD})/K_i(\text{hgal-1})$ . <sup>c</sup> Fc = ferrocenyl, [Ru] = ruthenium arene moiety, 3F-Ph = 3-fluorophenyl. <sup>d</sup> 2 $\beta$ -OMe denotes methyl *N*-acetyl- $\beta$ -lactosaminide (LacNAc1 $\beta$ -OMe).<sup>36</sup>

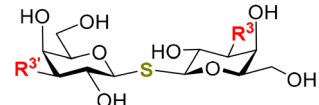
1–9). The selectivity was always in favor of *hgal*-3-CRD. The best improvement was obtained for compound **19** resulting from the attachment of ferrocenyltriazole to the 2-position of LacNAc. It bound *hgal*-3-CRD 13-fold more strongly than the parent methyl *N*-acetyl- $\beta$ -lactosaminide<sup>36</sup> 2 $\beta$ -OMe (entry 9). Complex **19** had affinity and selectivity comparable with that obtained for 5,6,7,8-tetrahydronaphthoate ester **43** (Fig. 3), which was among the most selective *hgal*-3 binders in a series of previously reported lactose 2-esters.<sup>49</sup> The remaining complexes **6**, **8**, **10**, and **16** had at most a two- to threefold improved affinity for both galectins relative to the parent disaccharides Lac (entries 4–6 vs. entry 1) and 2 $\beta$ -OMe (entry 8 vs.

entry 7). Ferrocenes **6** and **10** had only marginally better affinity for both *hgal*-1 and *hgal*-3-CRD than the non-metallic phenyl and hydroxymethyl compounds **7** and **4** (entries 4 and 6 vs. entries 3 and 2), respectively. Ruthenium arene **8** was a slightly weaker binder than the corresponding phenyl analog **7** (entries 5 and 3).

Next, we modified the 3'-position of the *N*-acetyl-lactosamine scaffold (compounds **25–30**, Table 1, entries 10–15), with the aim of introducing cation- $\pi$  interactions between Arg144 in subsite B of the *hgal*-3 CRD and the ferrocene/ruthenium arene complex attached to the 3'-position.<sup>12b,26a,50</sup> A similar approach has been used previously in the preparation of non-

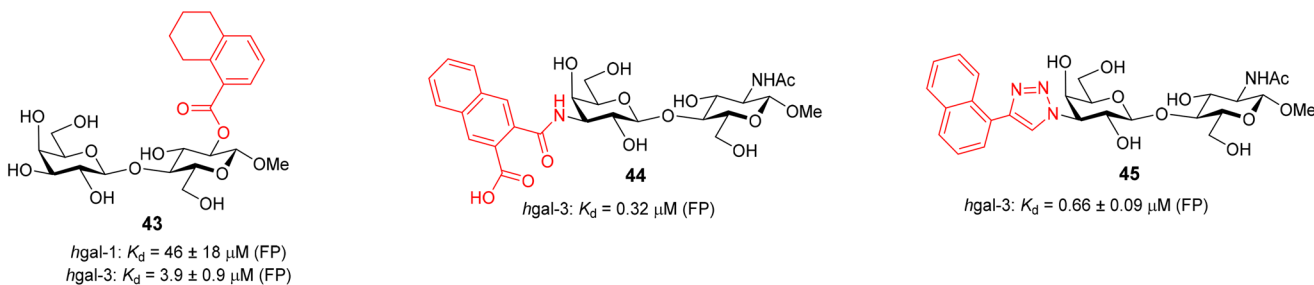




**Table 2** Apparent inhibition constant  $K_i$ , relative potency  $rp^a$  and selectivity values obtained from competitive fluorescence polarization for thiodigalactoside analogs<sup>b</sup>


Entry	R <sup>3</sup>	R <sup>3</sup>	Compound	$K_i$ ( <i>hgal</i> -1) ( $\mu$ M)	rp ( <i>hgal</i> -1)	$K_i$ ( <i>hgal</i> -3-CRD) ( $\mu$ M)	rp ( <i>hgal</i> -3-CRD)	Selectivity to <i>hgal</i> -1 <sup>c</sup>
1			<b>TD139</b>	$0.12 \pm 0.01$	1.00	$0.008 \pm 0.001$	1.00	0.07
2	OH		<b>34</b>	$1.9 \pm 0.2$	0.06	$1.7 \pm 0.4$	<0.01	0.89
3			<b>37</b>	$0.25 \pm 0.04$	0.48	$0.033 \pm 0.002$	0.24	0.13
4			<b>36</b>	$0.035 \pm 0.017$	<b>3.43</b>	$0.26 \pm 0.066$	<b>0.03</b>	<b>7.43</b>
5			<b>38</b>	$0.82 \pm 0.08$	0.15	$0.72 \pm 0.16$	0.01	0.88
6			<b>41</b>	$0.15 \pm 0.03$	<b>0.80</b>	$0.013 \pm 0.004$	<b>0.62</b>	<b>0.09</b>
7			<b>42</b>	$0.16 \pm 0.01$	0.75	$0.026 \pm 0.002$	0.31	0.16

<sup>a</sup> Relative potency with respect to **TD139**, one of the most potent inhibitor, defined as  $rp = K_i(\text{TD139})/K_i(\text{inhibitor})$ . <sup>b</sup> Fc = ferrocenyl, [Ru] = ruthenium arene moiety. <sup>c</sup> defined as the ratio  $K_i(\text{hgal-3-CRD})/K_i(\text{hgal-1})$ .

**Fig. 3** Structures of previously reported galectin inhibitors **43–45** and their affinities to *hgal*-1 and *hgal*-3 from FP.<sup>26a,49,50</sup> The affinity of **44** and **45** to *hgal*-1 was not reported.

organometallic *hgal*-3 inhibitors<sup>7d</sup> and resulted in affinities up to the high nanomolar range (see *N*-acetyllactosaminides **44** and **45** for examples, Fig. 3). Interestingly, the affinity for *hgal*-1 has not been previously determined for 3'-modified lactosamines. We found that 3-fluorophenyltriazole **28** (entry 12) and ruthenium arene **27** (entry 15) bound *hgal*-3-CRD approximately 7- and 5-fold more strongly than *hgal*-1, respectively, whereas the remaining 3'-modified lactosamine analogs displayed comparable or only 2- to 3-fold higher affinities for *hgal*-3-CRD than for *hgal*-1 despite the absence of an arginine residue in subsite B of *hgal*-1.

The 3'-hydroxymethyltriazole **29** (entry 10) bound both galectins better than the unmodified 2 $\beta$ -OMe due to the interaction of the triazole ring with the galectins.<sup>7d</sup> Substituting the hydroxymethyl group with phenyl in **26** significantly improved the affinity to the single-digit micromolar range. In agreement with the previous observations made for thiodigalactosides,<sup>14</sup> substituting fluorine for 3-hydrogen in the phenyl moiety of the analog **28** (entry 12) further increased the affinity, especially for *hgal*-3-CRD, which reached nanomolar values. Replacing the phenyl with ferrocene (**26**  $\rightarrow$  **25**, entry 13) resulted in an affinity comparable to that of the phenyl ana-



logue **26**, but for the first time in our series, the selectivity was very slightly tilted in favor of *hgal*-1. Substituting the bulky phthalimide in **30** (entry 14) for the acetamide in **25** (entry 13) further improved binding to *hgal*-3-CRD, producing the best inhibitor among our LacNAc- and Lac-based metal organocomplexes, probably owing to simultaneous interactions with subsites B and E. Disappointingly, the ruthenium arene complex **27** was a weaker inhibitor of both galectins compared with its ferrocene and phenyl counterparts **25** and **26**, respectively (entries 15 vs. 13 and 11).

Some thiodigalactoside-based inhibitors, such as compound **TD139**, are among the most potent *hgal*-1 and -3 inhibitors.<sup>14</sup> Also in this study, inhibitors resulting from the attachment of an organometallic substituent to the thiodigalactoside scaffold outperformed (Table 2) Lac- and LacNAc-derived inhibitors. Inhibitor **TD139** (entry 1) was more selective for *hgal*-3-CRD in our hands than originally reported. While the affinity for *hgal*-3-CRD ( $K_i = 0.008 \pm 0.001 \mu\text{M}$ ) was close to the reported value ( $K_i = 0.014 \pm 0.003 \mu\text{M}$ ),<sup>14</sup> the affinity for *hgal*-1 was one order of magnitude lower ( $K_i = 0.12 \pm 0.01 \mu\text{M}$ ) than originally reported ( $K_i = 0.012 \pm 0.003 \mu\text{M}$ ).<sup>14</sup> However, a value very close to ours was reported by Zetterberg *et al.* this year ( $K_i = 0.109 \pm 0.022 \mu\text{M}$  as determined by FP).<sup>13b</sup> Symmetrically substituted phenyltriazolyl-thiodigalactoside **37** was a selective *hgal*-3-CRD inhibitor, although less potent than **TD139** because it lacked the fluorine-galectin interactions contributing to the high binding affinity of **TD139** (Table 2, entries 1 and 3).<sup>14</sup> Substituting both planar phenyls in **37** with ferrocene to give **36** resulted in a significant drop in affinity toward *hgal*-3-CRD (almost by an order of magnitude, entries 3 and 4) and an improvement in affinity toward *hgal*-1. As a result, diferrocene **36** was the best and most selective organometallic inhibitor of *hgal*-1 in the series, because it bound *hgal*-1 7-fold more strongly than *hgal*-3-CRD, surpassing not only the diphenyl analog **37** (entries 3 and 4, 7-fold increase in affinity for *hgal*-1) but also the inhibitor **TD139** (entries 1 and 4, 3-fold increase), despite the absence of a fluorine substituent. The asymmetric monoferrocene complex **34** exhibited only micromolar affinity for both galectins (entry 2). The asymmetric ferrocene-phenyltriazole complexes **41** and **42** showed a good *hgal*-3-CRD selectivity (entries 6 and 7), although **42** bound *hgal*-3-CRD 3-fold more weakly than **TD139**. Ruthenium arene complex **38** (entry 5) displayed a significantly lower affinity for both galectins compared with its phenyl and ferrocenyl counterparts **37** and **36**, respectively, and was not further investigated.

**Intrinsic tryptophan fluorescence.** We determined the binding affinity expressed as a dissociation constant ( $K_d$ , Table 3) for selected ligands **6**, **19**, **25**, **27**, **28**, **36**, **37**, **41**, and **42** by an orthogonal method that utilizes ligand-induced changes in the intrinsic fluorescence of tryptophan residues.<sup>51</sup> Inhibitors **6**, **19**, and **25** (entries 3–5) represent the Lac and LacNAc scaffolds modified at the 1-, 2-, and 3'-positions, respectively. Inhibitor **36** was selected because it is the most potent and selective *hgal*-1 inhibitor in the whole series, whereas disaccharides **27**, **28**, **37**, **41**, and **42** were chosen because of their good selectivity in inhibition of *hgal*-3-CRD as

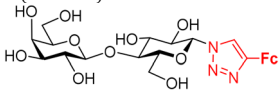
determined by fluorescence anisotropy. For comparison, the affinity of the endogenous ligands Lac and LacNAc and the known inhibitor **TD139** were also measured (Table 3, entries 1, 2, and 8). Unlike the competitive FP assay and ITC, which employed *hgal*-3-CRD to avoid *hgal*-3 oligomerization, this method has been also successfully applied to full-length *hgal*-3.<sup>51a</sup>

In all cases, the measured  $K_d$  to *hgal*-3-CRD was slightly lower than that obtained for full-length *hgal*-3; however, the difference did not appear significant in most cases, and the affinity trends were similar for both *hgal*-3 and *hgal*-3-CRD. Also, the values for disaccharides determined by the intrinsic tryptophan fluorescence assay and by the FP assay were comparable and did not differ by more than a factor of three in most cases. A more significant difference between the two methods was found for the potent *hgal*-1 inhibitor in the series **36** (Table 3, entry 10). The intrinsic tryptophan fluorescence assay indicated a higher affinity and selectivity of diferrocene **36** for *hgal*-1 than FP: Complex **36** bound *hgal*-1 50-fold more strongly than *hgal*-3, and 40-fold more strongly than *hgal*-3-CRD, whereas the selectivity using the FP assay was lower ( $(K_i(\textit{hgal}\text{-3-CRD})/K_i(\textit{hgal}\text{-1})) = 7.4$ ). The intrinsic tryptophan fluorescence assay also confirmed the selectivity of disaccharides **19**, **27**, **28**, **37**, **41**, **42** and **TD139** towards *hgal*-3. In contrast to the FP and ITC assays (see Table 4 for the ITC data), there was practically no difference between disaccharides **41** and **42** in binding to *hgal*-3, as both had low nanomolar affinity (Table 3, entries 11 and 12). This resulted in the 3-fluorophenyl analog **42** being a more selective *hgal*-3 inhibitor than the trifluorophenyl analog **41**, again in contrast to the FP results (Table 2, entries 6 and 7). Since these potent *hgal*-3 inhibitors **41** and **42** and *hgal*-1 inhibitor **36** carry an electroactive ferrocene moiety, we envision their application in electrochemical sensing of galectin inhibition. The commercial inhibitor **TD139** showed 4-fold higher *hgal*-3 affinity and 2-fold higher *hgal*-3 selectivity in the tryptophan fluorescence assay (Table 3, entry 8) than in the FP assay (Table 2, entry 1). Discrepancies between the two assays can be attributed to the different bioanalytical principles on which the assays are based. Importantly, both assays confirmed that the affinity and selectivity for *hgal*-1 were significantly improved by insertion of two ferrocene-triazole motifs into the thiodigalactoside scaffold to yield a potent *hgal*-1 inhibitor **36**.

**Chronopotentiometric stripping analysis.** We tested the formation of *hgal*-1 complex with selected ligands using chronopotentiometric stripping analysis (CPS),<sup>52</sup> in which proteins yield peak H. The structural transition between native and denatured forms of protein can be observed in dependence of peak H on stripping current  $I_{\text{STR}}$  (Fig. 4). The obtained result provides information whether the individual substances stabilize or destabilize the protein structure, which is manifested by a structural transition shift to lower or higher stripping current values.<sup>52</sup> *Hgal*-1 yielded a structural transition between  $I_{\text{STR}}$  of  $-17.5 \mu\text{A}$  and  $-30 \mu\text{A}$  with an  $I_{\text{STR}1/2}$  value<sup>53,54</sup> about  $-25 \mu\text{A}$ . The structural transition was accompanied by the splitting of a single peak H into two peaks characteristic of the



**Table 3** Dissociation constant  $K_d$  values obtained using intrinsic tryptophan fluorescence

Entry	Compounds	$K_d$ ( <i>hgal-1</i> ) ( $\mu\text{M}$ )	$K_d$ ( <i>hgal-3</i> ) ( $\mu\text{M}$ )	$K_d$ ( <i>hgal-3-CRD</i> ) ( $\mu\text{M}$ )	Selectivity to <i>hgal-1</i> <sup>a</sup>
1	<b>1</b> (Lac)	244 ± 29	297 ± 28	142 ± 23	1.2
2	<b>2</b> (LacNAc)	84 ± 13	80 ± 15	45 ± 12	0.9
3		193 ± 21	49 ± 8	30 ± 2	0.5
4	<b>6</b>	52 ± 4	5 ± 1	2.9 ± 0.3	0.1
5	<b>19</b>	1.8 ± 0.5	13 ± 2	8 ± 1	7.2
6	<b>25</b>	84 ± 12	10 ± 1	5.2 ± 0.5	0.12
7	<b>27</b>	2.2 ± 0.2	0.15 ± 0.03	0.08 ± 0.02	0.07
8	<b>28</b>	0.08 ± 0.01	0.0023 ± 0.0004	0.0021 ± 0.0004	0.03
9	<b>TD139</b>	0.12 ± 0.02	0.031 ± 0.004	0.012 ± 0.001	0.26
10	<b>37</b>	0.10 ± 0.001	0.50 ± 0.04	0.40 ± 0.10	50
11	<b>36</b>	0.035 ± 0.002	0.0067 ± 0.0006	0.0040 ± 0.0005	0.19
12	<b>41</b>	0.11 ± 0.01	0.0044 ± 0.0008	0.0038 ± 0.0006	0.04
	<b>42</b>				

<sup>a</sup> Defined as the ratio  $K_d(\textit{hgal-3})/K_d(\textit{hgal-1})$ .

Table 4 Thermodynamic parameters for binding to *hgal-1* and *hgal-3*-CRD obtained by ITC at  $T = 298$  K

Entry	Compound	$K_d$ ( $\mu\text{M}$ )	$\Delta G$ ( $\text{kcal mol}^{-1}$ )	$\Delta H$ ( $\text{kcal mol}^{-1}$ )	$-T\Delta S$ ( $\text{kcal mol}^{-1}$ )	$n$	Selectivity to <i>hgal-1</i> <sup>a</sup>
<i>hgal-1</i>							
1	<b>TD139</b> <sup>b</sup>	$0.220 \pm 0.05$	$-9.1 \pm 0.2$	$-16.7 \pm 0.4$	$7.6 \pm 0.4$	$0.96 \pm 0.04$	0.31
2	<b>TD139</b>	$0.279 \pm 0.001$	$-8.9 \pm 0.1$	$-16.9 \pm 0.4$	$8.0 \pm 0.4$	$1.03 \pm 0.04$	0.07
3	<b>37</b>	$0.288 \pm 0.006$	$-8.9 \pm 0.1$	$-9.6 \pm 0.4$	$0.7 \pm 0.4$	$1.04 \pm 0.02$	0.33
4	<b>36</b>	$0.258 \pm 0.004$	$-9.0 \pm 0.1$	$-12.8 \pm 1.4$	$3.8 \pm 1.5$	$1.06 \pm 0.07$	3.6
5	<b>41</b>	$0.340 \pm 0.019$	$-8.9 \pm 0.1$	$-10.2 \pm 0.1$	$1.3 \pm 0.1$	$1.03 \pm 0.00$	0.07
6	<b>42</b>	$0.366 \pm 0.031$	$-8.8 \pm 0.1$	$-9.5 \pm 0.1$	$0.6 \pm 0.1$	$1.03 \pm 0.02$	0.18
<i>hgal-3</i> -CRD							
7	<b>TD139</b> <sup>b</sup>	$0.068 \pm 0.01$	$-9.9 \pm 0.4$	$-18.2 \pm 0.8$	$8.3 \pm 0.9$	$0.96 \pm 0.01$	—
8	<b>TD139</b>	$0.019 \pm 0.003$	$-10.6 \pm 0.1$	$-16.4 \pm 0.4$	$5.8 \pm 0.3$	$1.08 \pm 0.01$	—
9	<b>37</b>	$0.096 \pm 0.005$	$-9.6 \pm 0.1$	$-11.2 \pm 0.3$	$1.7 \pm 0.2$	$1.03 \pm 0.03$	—
10	<b>36</b>	$0.923 \pm 0.040$	$-8.3 \pm 0.1$	$-12.7 \pm 0.2$	$4.4 \pm 0.1$	$1.08 \pm 0.02$	—
11	<b>41</b>	$0.023 \pm 0.006$	$-10.5 \pm 0.2$	$-14.0 \pm 1.3$	$3.6 \pm 1.5$	$1.03 \pm 0.04$	—
12	<b>42</b>	$0.066 \pm 0.010$	$-9.8 \pm 0.1$	$-12.0 \pm 0.2$	$2.3 \pm 0.4$	$1.01 \pm 0.00$	—

<sup>a</sup> Defined as the ratio  $K_d(\textit{hgal-3})/K_d(\textit{hgal-1})$ . <sup>b</sup> Taken from ref. 12b.

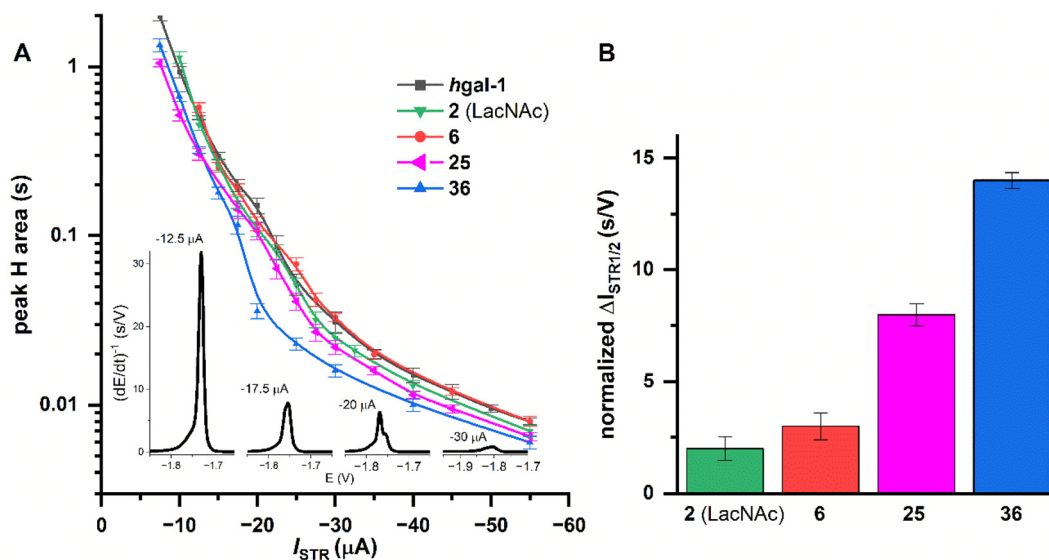


Fig. 4 (A) The dependence of peak H area on stripping current  $I_{\text{STR}}$  for free *hgal-1* (grey) and that in complex with compounds **2** (green), **6** (red), **25** (magenta), and **36** (blue). Inset: peak H height of free *hgal-1* measured using different stripping currents. A double peak of structural transition can be seen at  $-20$   $\mu\text{A}$ . (B)  $\Delta I_{\text{STR}1/2}$  values of *hgal-1* complexes normalized<sup>52b</sup> to free *hgal-1*.

native and denatured *hgal-1* (Fig. 4A, inset). Interaction with LacNAc (**2**) and compounds **6**, **25**, and **36** shifted the structural transition characterized by  $I_{\text{STR}1/2}$  to lower values, indicating the stabilization of *hgal-1* molecules against the effect of the electric field. The average values of this structural transition shift for *hgal-1* in complex with disaccharides compared to those of free *hgal-1* are in good agreement with the results

(binding affinities) obtained by other methods, giving the lowest  $\Delta I_{\text{STR}1/2}$  value for the strongest binder **36** (Fig. 4B). However, the determination of  $I_{\text{STR}1/2}$  for *hgal-1* interaction with compounds **2** and **6** is within the experimental limits of the CPS method.

**Isothermal titration microcalorimetry (ITC).** Ferrocene-modified thiodigalactosides emerged as the most potent



organometallic inhibitors tested in this study. To assess how the substitution of ferrocene for the phenyl and fluorophenyl groups affects the thermodynamics of binding in the thiodigalactoside series, we determined the thermodynamic binding parameters (Table 4 and Fig. 5) of five TDG analogs, three symmetrically substituted thiodigalactoside-based inhibitors, namely bis(3-fluorophenyl) inhibitor **TD139**, and its diphenyl and diferrocene analogs **37** and **36**, and two asymmetrically substituted thiodigalactosides, trifluorophenyl-ferrocenyl inhibitor **41** and 3-fluorophenyl-ferrocenyl analog **42**. We used *hgal-3*-CRD instead of complete *hgal-3* to minimize complications resulting from oligomerization of *hgal-3*.<sup>16</sup> The ITC measurement yielded lower affinities than FP and intrinsic tryptophan fluorescence, but this phenomenon has been reported previously for galectin inhibitors including **TD139**.<sup>12b</sup> The data for binding of **TD139** to *hgal-1* were essentially identical to those recently reported (Table 4, entries 1 and 2),<sup>12b</sup> whereas the binding affinity for *hgal-3*-CRD was approximately 3.6-fold higher in our hands than that reported<sup>12b</sup> but still comparable (entries 7 and 8). The ITC assay confirmed the selectivity of the diferrocene inhibitor **36** towards *hgal-1*, albeit with a lower selectivity value of 3.6 (entries 4 and 10), than that determined by FP (7.4) and intrinsic tryptophan fluorescence (40). ITC also confirmed the *hgal-3* selectivity of the asymmetrically substituted thiodigalactosides **41** and **42**, which exhibited selectivity values comparable to those obtained by FP (entries 5, 6, 11, and 12).

The ITC data confirmed that the binding affinity for *hgal-3*-CRD decreased when moving from the bis(fluorophenyl) analog **TD139** to the diphenyl analog **37** and the diferrocene analog **36** (Table 4, entries 8–10). This trend was consistent with the FP assay. Compared to diphenyl analog **37** (entry 3), bis(fluorophenyl) inhibitor **TD139** (entry 2) displayed a higher

binding enthalpy to *hgal-1* ( $-16.9$  vs.  $-9.6$  kcal mol<sup>-1</sup>) accompanied by a significant increase in the entropic penalty ( $8.0$  vs.  $0.7$  kcal mol<sup>-1</sup>), leading to a perfect enthalpy-entropy compensation with a negligible change in affinity for *hgal-1*. Binding of **TD139** to *hgal-3*-CRD also showed a gain in enthalpy relative to diphenyl analog **37** (entries 8 and 9,  $-16.4$  vs.  $-11.2$  kcal mol<sup>-1</sup>). However, the increased entropic penalty ( $5.8$  vs.  $1.7$  kcal mol<sup>-1</sup>) did not fully compensate for this gain, resulting in a higher overall affinity of **TD139** to *hgal-3*-CRD. Thus, the ITC data suggests that while the fluorine substituent in **TD139** interacts with the protein backbone in both galectins,<sup>12b</sup> it produces a significant gain in affinity only in the case of *hgal-3*-CRD. This is probably due to better protein preorganization.

For the diferrocene complex **36**, the higher enthalpy of binding to *hgal-1* compared to its diphenyl analog **37** ( $-12.8$  vs.  $-9.6$  kcal mol<sup>-1</sup>) was completely compensated for by the increased entropic penalty of **36** ( $3.8$  vs.  $0.7$  kcal mol<sup>-1</sup>) leading to virtually identical binding affinities of compounds **36** and **37** for *hgal-1* (entries 3 and 4). In contrast, the entropic penalty of diferrocene **36** relative to its diphenyl counterpart **37** ( $4.4$  vs.  $1.7$  kcal mol<sup>-1</sup>) exceeded the enthalpy gain ( $-12.7$  vs.  $-11.2$  kcal mol<sup>-1</sup>) in binding to *hgal-3*-CRD, resulting in a significantly lower affinity of **36** for this galectin (entries 9 and 10), and hence selectivity for *hgal-1* over *hgal-3*. We interpret these ITC data in terms of an entropically unfavorable structural transition that *hgal-3*-CRD has to undergo to accommodate the bulky ferrocene moiety, which outweighs any attractive interaction. Asymmetrically substituted mono-ferrocene analogs **41** and **42** showed binding behavior similar to **TD139**, with significantly higher affinity for *hgal-3*-CRD than for *hgal-1* (Table 4, entries 5, 6, 11, and 12), suggesting that *hgal-3*-CRD accommodates one ferrocene group in inhibitors **41** or **42**

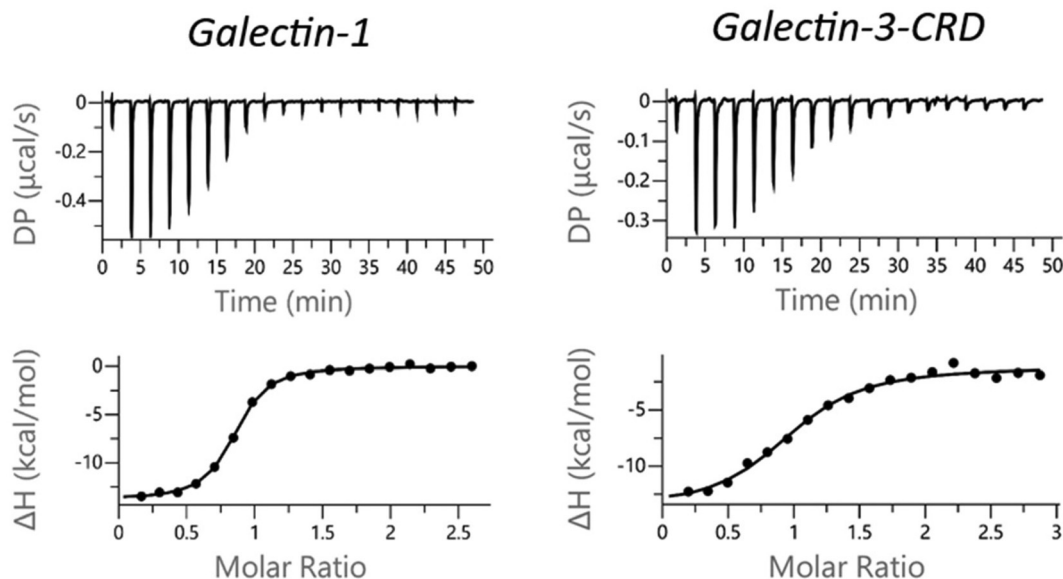


Fig. 5 Thermograms and binding isotherms obtained by isothermal titration calorimetry for the interaction of **36** with *hgal-1* and *hgal-3*-CRD.



more effectively than two ferrocenes in compound **36**. This was further investigated by computational modeling and  $^{19}\text{F}$  NMR spectroscopy.

#### Computational modelling of ligand-galectin interactions.

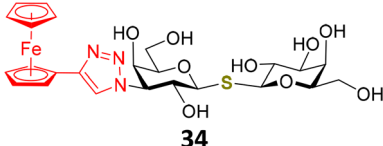
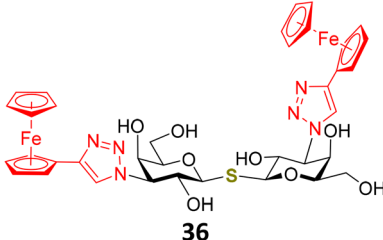
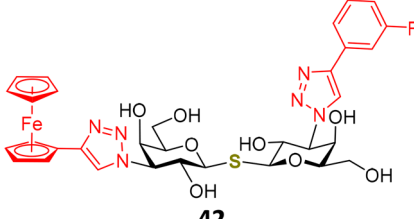
The asymmetric monoferrocene complex **34** exhibited only a micromolar and essentially identical affinity for both galectins (Table 2, entry 2). Because the symmetrical diferrocene complex **36** exhibited a 54-fold increase in affinity toward *hgal*-1 but only a 7-fold increase toward *hgal*-3-CRD compared to **34**, it seems likely that the symmetrically placed ferrocene moieties in inhibitor **36** can interact more efficiently with subsites A/B and E in *hgal*-1 than in *hgal*-3-CRD. To evaluate possible interactions between the ferrocene group and these subsites and to compare them with those of the planar fluorophenyl group, we attempted to estimate the binding energies of mono- and diferrocene analogs **34** and **36**, respectively, and fluorophenyl ferrocene analog **42** for *hgal*-1 and *hgal*-3-CRD using molecular modeling tools (Table 5). For the calculation, we used a simple model based on a combination of molecular dynamics of the ligand-galectin complex and subsequent estimation of the ligand binding enthalpy for a set of sampled MD geometries. MD simulations were performed in Desmond,<sup>55,56</sup> and binding enthalpies were calculated at the semiempirical level in MOPAC.<sup>57</sup> (see ESI† for a detailed method description). Table 5 summarizes the computationally estimated binding enthalpies for disaccharides **34**, **36**, and **42**. Because of the asymmetric character of compounds **34** and **42**, two binding modes were considered. In the first binding mode, the ferrocene moiety is positioned in subsites A and B

of a galectin. In the second mode, it resides in the E subsite (Fig. 6 and Fig. S80–S83 in ESI†). Only one binding mode was considered for diferrocene **36** (Fig. S78–S79 in ESI†) because of its symmetry. It is obvious from the comparison of the calculated  $\Delta H_{\text{bind}}$  (Table 5, entries 3–5) and experimentally determined  $\Delta H$  for diferrocene **36** (Table 4, entries 4 and 10) and mono-ferrocene **42** (entries 6 and 12) that the calculation overestimates binding enthalpies (see discussion in ESI, pp. S81–S82†).

Notwithstanding the aforementioned inaccuracies and the absence of the entropic penalty from the calculations, the determined binding enthalpies correlated consistently with the experimentally determined affinities. Accordingly, complex **36** demonstrated the highest binding enthalpy of all calculated disaccharides in binding to *hgal*-1 ( $-34.1$  kcal mol<sup>-1</sup>), along with relatively strong binding to *hgal*-3-CRD ( $-30.4$  kcal mol<sup>-1</sup>). These results are consistent with the ITC data, where complex **36** displayed a similar enthalpy change in binding to both galectins, whereas the decrease in affinity to *hgal*-3-CRD stemmed from a higher entropic penalty (Table 4, entries 4 and 10). Notably, complexes **34** and **42** exhibited significantly higher binding enthalpies in binding to *hgal*-1 when the ferrocene moiety occupied subsites A and B. Conversely, the preferred binding mode of these complexes to *hgal*-3-CRD positioned the ferrocene moiety in subsite E. Thus, the MD simulation suggests that *hgal*-1 accommodates the bulky ferrocene moiety in subsites A and B more efficiently than *hgal*-3-CRD.

**Monitoring of the  $^{19}\text{F}$  { $^1\text{H}$ } resonances of the 3-fluorophenyl moiety.** The presence of the fluorine atom in compounds **28**,

Table 5 Binding enthalpy calculated from MD simulation

Entry	Compounds	Binding mode (subsites in which the ferrocene moiety is positioned)	$\Delta H_{\text{bind}}$ (kcal mol <sup>-1</sup> ) <i>hgal</i> -1	$\Delta H_{\text{bind}}$ (kcal mol <sup>-1</sup> ) <i>hgal</i> -3-CRD
1	 <b>34</b>	A and B (Fig. 6A and C)	-16.9	-16.3
2		E (Fig. 6B and D)	-8.4	-25.8
3	 <b>36</b>	A and B, and E (Fig. S78–S79 in ESI†)	-34.1	-30.4
4		A and B (Fig. S80 and S82 in ESI†)	-32.3	-30.4
5	 <b>42</b>	E (Fig. S81 and S83 in ESI†)	-27.3	-32.9



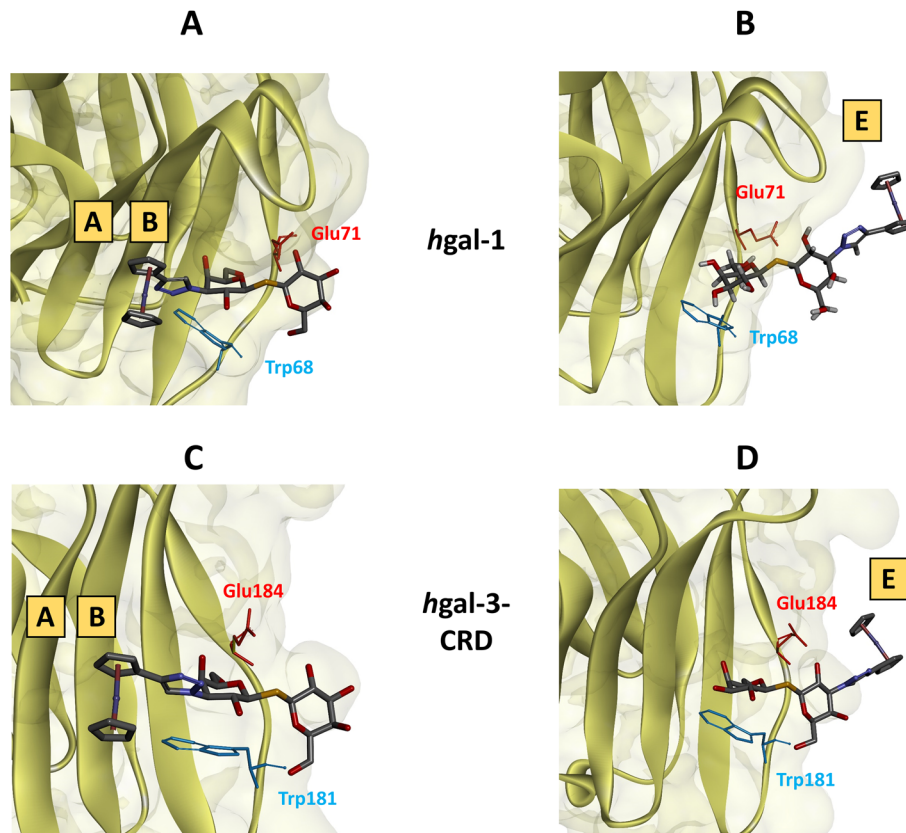


**Fig. 6** Geometries of compound **34** bound to *hgal-1* or *-3-CRD* derived from molecular dynamics calculations showing characteristic amino acid residues (Glu71 and Trp68 for *hgal-1*, Glu184 and Trp181 for *hgal-3-CRD*) interacting with the hexopyranose rings. (A) Ferrocene moiety in subsites A and B of *hgal-1*. (B) Ferrocene moiety is in subsite E of *hgal-1*. (C) Ferrocene moiety in subsites A and B of *hgal-3-CRD*. (D) Ferrocene moiety in subsite E of *hgal-3-CRD*.

**42**, and **TD139** enabled us to use sensitive  $^{19}\text{F}\{^1\text{H}\}$  NMR experiments to map the position of the 3-fluorophenyl-triazole moiety in both galectins. All investigated compounds **TD139**, **28**, and **42** showed a single sharp  $^{19}\text{F}$  resonance close to  $-114$  ppm in the unbound state (Fig. S84 in ESI $^\dagger$ ). According to a previous report, the interaction of **TD139** with either *hgal-1* or *hgal-3-CRD* resulted in similar  $^{19}\text{F}$  NMR spectra revealing multiple resonances of the galectin-bound states in slow chemical exchange.<sup>12b</sup> In our hands, measuring the solution of **TD139** with the excess of either *hgal-1* or *hgal-3-CRD* relative to the ligand produced two bound state  $^{19}\text{F}$ -NMR resonances (Fig. 7, red spectra). Repetition of the experiment with an excess of **TD139** relative to the galectins showed an additional resonance of unbound **TD139**, distinct from the bound state signals (Fig. S85 and S88 in ESI $^\dagger$ ).

To facilitate the interpretation of the  $^{19}\text{F}\{^1\text{H}\}$  NMR spectra of protein-bound **TD139**, we performed the same NMR experiments with 3'-fluorophenyl *N*-acetylglucosamine **28**. This ligand showed only one  $^{19}\text{F}$  resonance of its bound state upon addition of either *hgal-1* or *hgal-3-CRD* (Fig. 7 blue spectra, Fig. S86 and S89 in ESI $^\dagger$ ). Because disaccharide **28** is an unsymmetrical LacNAc analog, the galactopyranoside ring can only occupy subsite C with the 3'-fluorophenyl ring pointing

toward subsites A/B.<sup>7b,12a,50,58</sup> Therefore, its  $^{19}\text{F}$  resonance was assigned to the fluorophenyl-triazole group located in subsites A/B. The chemical shift of the bound state  $^{19}\text{F}$  resonance in compound **28** closely matched one of the two resonances of bound **TD139** in the presence of either *hgal-1* or *hgal-3-CRD* (Fig. 7 red vs. blue spectra). Therefore, this resonance of **TD139** was also assigned to the fluorophenyl-triazole group positioned in subsites A/B. Consequently, the remaining broad signal at  $\delta = -115.01$  ppm of **TD139** bound to *hgal-1* (Fig. 7, *hgal-1*, pink label) was assigned to the fluorophenyl moiety occupying subsite E. Similarly, the more downfield-shifted  $^{19}\text{F}$  resonance of **TD139** bound to the *hgal-3-CRD* (Fig. 7, *hgal-3-CRD*, pink label) was also assigned to the fluorophenyl-triazole moiety in subsite E. It should be noted that this assignment is based on the assumption that the differences between the compounds **28** and **TD139** do not affect the interactions of the fluorine atom with the binding subsites A/B or E and thus its chemical shift in these subsites.

In principle, the ferrocene moiety in compound **42** can occupy subsites A/B, or subsite E in both galectins, leading to two distinct binding modes (Fig. 6). Indeed, the  $^{19}\text{F}\{^1\text{H}\}$  NMR spectrum of **42** in the presence of *hgal-1* showed two bound state  $^{19}\text{F}$  NMR signals (Fig. 7, *hgal-1*, green spectrum, Fig. S87



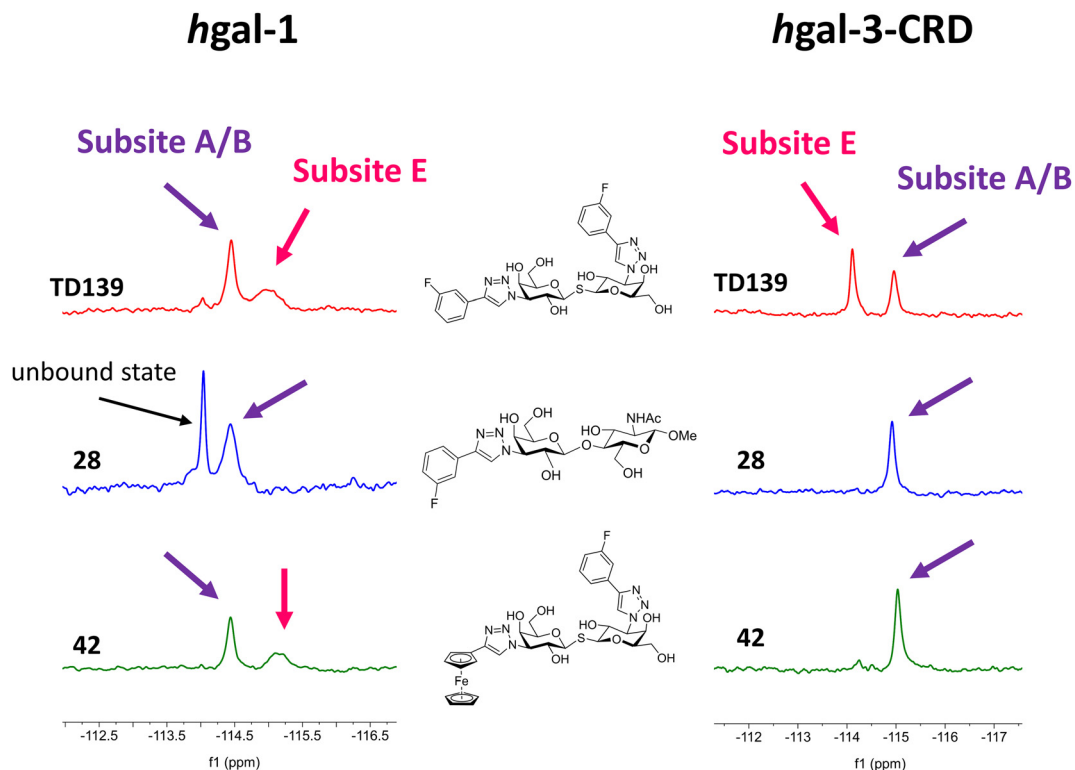


**Fig. 7**  $^{19}\text{F}\{^1\text{H}\}$  NMR spectra of ligands **28**, **42**, and **TD139** in the presence of *hgal-1* or *hgal-3-CRD*, pink arrows indicate resonances of fluorine in subsite E, purple arrows indicate resonances of fluorine in subsites A/B. Except for the combination **28** with *hgal-1*, all these spectra were acquired using an excess of the galectin over the ligand.

in ESI $^+$ ), whose chemical shifts matched the two bound state resonances of **TD139** with *hgal-1* (Fig. 7, *hgal-1*, red spectrum). Therefore, the fluorophenyl group in **42** occupies both subsites

A/B and subsite E during recognition by *hgal-1*, and consequently the ferrocene group is likely to occupy these two subsites as well. Conversely, disaccharide **42** exhibited only a

**Table 6**  $IC_{50}$  [ $\mu\text{M}$ ] values obtained by the MTT assay after 72 h treatment of cells with selected compounds<sup>a</sup>

Entry	Compound	A2780	SK-OV-3	MDA-MB-231	HEK-293
1	<b>6</b> (Lac1 $\beta$ -Fc')	85 $\pm$ 8	>200	183 $\pm$ 35	>200
2	<b>8</b> (Lac1 $\beta$ -Ru')	69 $\pm$ 12	>200	>200	>200
3	<b>10</b> (Lac1 $\beta$ -OCH <sub>2</sub> CH <sub>2</sub> Fc')	116 $\pm$ 14	>200	170 $\pm$ 5	198 $\pm$ 35
4	<b>16</b> (LacNAc1 $\beta$ -Fc')	>200	>200	>200	>200
5	<b>19</b> (2-Fc'-Lac1 $\beta$ -OMe)	159 $\pm$ 54	>200	>200	>200
6	<b>25</b> (3'-Fc'-LacNAc1 $\beta$ -OMe)	>200	>200	>200	>200
7	<b>27</b> (3'-Ru'-LacNAc1 $\beta$ -OMe)	161 $\pm$ 50	>200	>200	143 $\pm$ 44
8	<b>30</b> (3'-Fc'-LacNPhth1 $\beta$ -OMe)	>200	>200	>200	>200
9	<b>34</b> (3'-Fc'-TDG)	90 $\pm$ 5	>200	>200	>200
10	<b>36</b> (3,3'-diFc'-TDG)	>200	>200	>200	151 $\pm$ 11
11	<b>38</b> (3,3'-diRu'-TDG)	>200	>200	125 $\pm$ 21	>200
12	<b>41</b> (3-F <sub>3</sub> Ph-3'-Fc'-TDG)	168 $\pm$ 8	>200	>200	152 $\pm$ 6
13	<b>42</b> (3-3FPPh-3'-Fc'-TDG)	>200	>200	>200	>200
14	<b>cisPt</b>	1.7 $\pm$ 0.3	5.6 $\pm$ 1.0	3.8 $\pm$ 0.5	3.7 $\pm$ 0.6

<sup>a</sup>To facilitate orientation, the structures of compounds are indicated using the abbreviations Lac, LacNAc, and TDG for the disaccharides, and abbreviations Fc', Ru', 3FPPh, and F<sub>3</sub>Ph for the triazole-linked moieties as defined below the Table heading.





single bound state  $^{19}\text{F}$  resonance (Fig. 7, *hgal*-3-CRD, green spectrum, Fig. S90 in ESI†) in the presence of *hgal*-3-CRD, similar to compound **28** (Fig. 7, *hgal*-3-CRD, blue spectrum), suggesting that the fluorophenyl substituent of **42** interacts only with subsites A/B during recognition by *hgal*-3-CRD. Thus, the bulky ferrocene moiety is unlikely to occupy subsites A/B in *hgal*-3-CRD and compound **42** prefers to bind *hgal*-3-CRD through the binding mode with the ferrocene moiety located in subsite E, which is consistent with computational modeling (Table 5, entries 4 and 5).

### Cytotoxicity

Ferrocene itself is not significantly toxic.<sup>20b</sup> Compounds formed by the insertion of ferrocene into bioactive compounds to enhance a particular bioactivity generally showed low toxicity.<sup>59</sup> However, we can also find examples of highly cytotoxic ferrocene compounds<sup>60</sup> including ferrocene-containing glycomimetics.<sup>61</sup> Therefore, we screened the *in vitro* cytotoxicity of the prepared organometallic hybrid inhibitors against human ovarian cancer cell lines A2780 and SK-OV-3, human triple-negative breast cancer cell line MDA-MB-231, and human embryonic kidney non-malignant cell line HEK-293. A MTT cell viability assay was performed after 72 h of treatment and cell viability was expressed as  $IC_{50}$  values (Table 6). In this initial screening, we did not attempt to correlate the cytotoxicity of inhibitors with galectin expression in the cells, which is reserved for a detailed follow-up study. The tested disaccharides showed minimal or only weak cytotoxicity towards the cancer cell lines SK-OV-3, MDA-MB-231, and the non-malignant HEK-293. Complexes **6**, **8** and **34** exhibited moderate cytotoxicity towards A2780 cell line (Table 6, entries 1, 2, and 9). Notably, the potent inhibitors **36**, **41** and **42** showed no significant cytotoxicity (entries 10, 12, and 13).

### Conclusion

This study reports a novel approach to the design of galectin inhibitors using disaccharides modified with ferrocenes and ruthenium arenes. We have thoroughly investigated their binding to *hgal*-1 and *hgal*-3-CRD through a series of binding assays and experiments, including fluorescence anisotropy, intrinsic fluorescence of the tryptophan residues, chronopotentiometric stripping analysis, isothermal titration microcalorimetry, molecular dynamics simulation, and the monitoring of  $^{19}\text{F}\{^1\text{H}\}$  NMR resonances. Disaccharides containing a ruthenium arene complex were found to be weaker galectin binders than the corresponding ferrocene analogs. The inhibitors interacting with the galectin subsite E *via* the ferrocene moiety (Lac and LacNAc modified at the 1- or 2-position) exhibited an increase in affinity to both galectins similar to that observed for inhibitors with planar organic arenes at the corresponding disaccharide positions. However, the attachment of ferrocene to positions 3/3' of the galactopyranoside ring significantly enhanced the affinity for both disaccharide scaffolds tested,

*N*-acetylglucosamine and thiodigalactoside, and in the case of diferrocenyl-thiodigalactoside **36**, surpassed the performance of the inhibitors possessing planar arenes, leading to a reversal of the inhibitor selectivity in favor of *hgal*-1 over *hgal*-3.

Notably, the thiodigalactoside-based diferrocene inhibitor **36** proved to be a potent and selective *hgal*-1 inhibitor whereas thiodigalactoside analogs **41** and **42**, which incorporate only a single ferrocene moiety, showed good affinity and selectivity for *hgal*-3 comparable to **TD139**. A preliminary hypothesis based on molecular dynamics simulations and the measurement of  $^{19}\text{F}\{^1\text{H}\}$  NMR resonances attributed the selectivity of inhibitor **36** to the restrictions imposed by the ferrocene moiety when binding to *hgal*-3-CRD. Further experiments to elucidate the molecular basis of the unusual affinity and selectivity of this inhibitor are underway in our group. We also envisage that the series of ferrocene-containing inhibitors with varying affinities developed in this study can be used to exploit the electrochemical activity of the ferrocene moiety for the development of an electrochemical galectin binding assay, an avenue currently under active investigation in our group.

### Author contributions

Vojtěch Hamala and Martin Kurfiřt contributed equally to this study. Vojtěch Hamala: conceptualization, investigation (synthesis), data curation and writing – original draft. Martin Kurfiřt: investigation (synthesis,  $^{19}\text{F}$  NMR experiments) and data curation. Lucie Červenková Šťastná and Jana Bernášková: investigation (NMR and HRMS analysis). Hedvika Hujerová: investigation (synthesis). Kamil Parkan: investigation (fluorescence probe synthesis). Jakub Kaminský: investigation (molecular modelling). Nina Habanová: investigation ( $^{19}\text{F}$  NMR experiments). Jaroslav Kozák and Alžběta Magdolenová: investigation (fluorescence polarization). Martin Zavřel and Jitka Holčáková: investigation (galectins cloning and purification). Tatiana Staroňová, Veronika Ostatná, Lucie Žaloudková and Aleš Daňhel: investigation (voltammetric analysis, tryptophan fluorescence assay and chronopotentiometric stripping analysis). Petr Voňka: investigation (isothermal titration microcalorimetry). Roman Hrstka: funding acquisition, investigation and supervision. Jindřich Karban: conceptualization, funding acquisition, investigation, project administration, supervision, writing – review & editing.

### Data availability

The data supporting this article have been included as part of the ESI.†

### Conflicts of interest

The authors declare no conflict of interest.



## Acknowledgements

The financial support of The Czech Science Foundation is gratefully acknowledged (Grant No. 23-06115S). This work was financially supported from Specific University Research (grant No. A1 FPBT 2023 003) and by Ministry of Health, Czech Republic – conceptual development of research organization (MMCI, 00209805). The research was also supported by the project National Institute for Cancer Research (Programme EXCELES, ID Project No. LX22NPO5102) – Funded by the European Union – Next Generation EU. We also appreciate the support from Gilead Sciences, Inc., provided under the program ‘Molecules for Life’ at the Gilead Sciences & IOCB Prague Research Centre. Computational resources have been provided by the e-INFRA CZ project (ID: 90254), supported by the Ministry of Education, Youth and Sports of the Czech Republic and by the ELIXIR-CZ project (ID: 90255), part of the international ELIXIR infrastructure. Vojtech Hamala is grateful for the financial support of the Martina Roeselová Memorial Fellowship granted by the IOCB Tech Foundation. The author extends gratitude to Petr Páchl from IOCB Prague for his work on cloning and purifying human galectin-1 for the fluorescence polarization assay.

## References

- H.-J. Gabius, M. Cudic, T. Diercks, H. Kaltner, J. Kopitz, K. H. Mayo, P. V. Murphy, S. Oscarson, R. Roy, A. Schedlbauer, S. Toegel and A. Romero, What is the Sugar Code?, *ChemBioChem*, 2022, **23**(13), e202100327.
- (a) H. Rachel and L. Chang-Chun, Chapter 5 - Recent advances toward the development of inhibitors to attenuate tumor metastasis via the interruption of lectin–ligand interactions, in *Adv. Carbohydr. Chem. Biochem*, ed. D. Horton, Academic Press, 2013, vol. 69, pp. 125–207; (b) B. A. H. Smith and C. R. Bertozzi, The clinical impact of glycobiology: targeting selectins, Siglecs and mammalian glycans, *Nat. Rev. Drug Discovery*, 2021, **20**(3), 217–243.
- (a) B. Ernst and J. L. Magnani, From carbohydrate leads to glycomimetic drugs, *Nat. Rev. Drug Discovery*, 2009, **8**(8), 661–677; (b) J. Aretz, E.-C. Wamhoff, J. Hanske, D. Heymann and C. Rademacher, Computational and Experimental Prediction of Human C-Type Lectin Receptor Druggability, *Front. Immunol.*, 2014, **5**, 323; (c) E. Shanina, S. Kuhaudomlarp, E. Siebs, F. F. Fuchsberger, M. Denis, P. da Silva Figueiredo Celestino Gomes, M. H. Clausen, P. H. Seeberger, D. Rognan, A. Titz, A. Imberty and C. Rademacher, Targeting undruggable carbohydrate recognition sites through focused fragment library design, *Commun. Chem.*, 2022, **5**(1), 64.
- (a) M. Agostino, E. Yuriev and P. A. Ramsland, A Computational Approach for Exploring Carbohydrate Recognition by Lectins in Innate Immunity, *Front. Immunol.*, 2011, **2**, 23; (b) S. Leusmann, P. Menova, E. Shanin, A. Titz and C. Rademacher, Glycomimetics for the inhibition and modulation of lectins, *Chem. Soc. Rev.*, 2023, **52**(11), 3663–3740; (c) C. P. Modenutti, J. I. B. Capurro, S. Di Lella and M. A. Martí, The Structural Biology of Galectin-Ligand Recognition: Current Advances in Modeling Tools, Protein Engineering, and Inhibitor Design, *Front. Chem.*, 2019, **7**, 823; (d) R. Hevey, Strategies for the Development of Glycomimetic Drug Candidates, *Pharmaceuticals*, 2019, **12**(2), 55.
- V. C. Damalanka, A. R. Maddirala and J. W. Janetka, Novel approaches to glycomimetic design: development of small molecular weight lectin antagonists, *Expert Opin. Drug Discovery*, 2021, **16**(5), 513–536.
- L. Johannes, R. Jacob and H. Leffler, Galectins at a glance, *J. Cell Sci.*, 2018, **131**(9), jcs208884.
- (a) Y.-C. Chan, H.-Y. Lin, Z. Tu, Y.-H. Kuo, S.-T. D. Hsu and C.-H. Lin, Dissecting the Structure–Activity Relationship of Galectin–Ligand Interactions, *Int. J. Mol. Sci.*, 2018, **19**(2), 392; (b) S. Bertuzzi, J. I. Quintana, A. Ardá, A. Gimeno and J. Jiménez-Barbero, Targeting Galectins With Glycomimetics, *Front. Chem.*, 2020, **8**, 593; (c) C. Porciúncula-González, A. J. Cagnoni, C. Fontana, K. V. Mariño, P. Saenz-Méndez, C. Giacomini and G. Irazoqui, Structural insights in galectin-1-glycan recognition: Relevance of the glycosidic linkage and the N-acetylation pattern of sugar moieties, *Biorg. Med. Chem.*, 2021, **44**, 116309; (d) C. T. Öberg, H. Leffler and U. J. Nilsson, Inhibition of Galectins with Small Molecules, *Chim. Int. J. Chem.*, 2011, **65**(1), 18–23.
- V. Denavit, D. Lainé, T. Tremblay, J. St-Gelais and D. Giguère, Synthetic Inhibitors of Galectins: Structures and Syntheses, *Trends Glycosci. Glycotechnol.*, 2018, **30**(172), SE21–SE40.
- (a) R. M. Perrotta, C. A. Bach, M. Salatino and G. A. Rabinovich, Reprogramming the tumor metastasis cascade by targeting galectin-driven networks, *Biochem. J.*, 2021, **478**(3), 597–617; (b) C.-H. Li, Y.-C. Chang, M.-H. Chan, Y.-F. Yang, S.-M. Liang and M. Hsiao, Galectins in Cancer and the Microenvironment: Functional Roles, Therapeutic Developments, and Perspectives, *Biomedicine*, 2021, **9**(9), 1159; (c) K. V. Mariño, A. J. Cagnoni, D. O. Croci and G. A. Rabinovich, Targeting galectin-driven regulatory circuits in cancer and fibrosis, *Nat. Rev. Drug Discovery*, 2023, **22**(4), 295–316.
- D. J. Laderach and D. Compagno, Inhibition of galectins in cancer: Biological challenges for their clinical application, *Front. Immunol.*, 2023, **13**, 1104625.
- C. M. Arthur, M. D. Baruffi, R. D. Cummings and S. R. Stowell, Evolving Mechanistic Insights into Galectin Functions, in *Galectins: Methods and Protocols*, ed. S. R. Stowell, R. D. Cummings, Springer New York, New York, NY, 2015, pp. 1–35.
- (a) M. F. López-Lucendo, D. Solís, S. André, J. Hirabayashi, K.-i. Kasai, H. Kaltner, H.-J. Gabius and A. Romero, Growth-regulatory Human Galectin-1: Crystallographic Characterisation of the Structural Changes Induced by Single-site Mutations and their Impact on the Thermodynamics of Ligand Binding, *J. Mol. Biol.*, 2004,



- 343(4), 957–970; (b) T.-J. Hsieh, H.-Y. Lin, Z. Tu, T.-C. Lin, S.-C. Wu, Y.-Y. Tseng, F.-T. Liu, S.-T. D. Hsu and C.-H. Lin, Dual thio-digalactoside-binding modes of human galectins as the structural basis for the design of potent and selective inhibitors, *Sci. Rep.*, 2016, **6**(1), 29457.
- 13 (a) K. Peterson, P. M. Collins, X. Huang, B. Kahl-Knutsson, S. Essén, F. R. Zetterberg, S. Oredsson, H. Leffler, H. Blanchard and U. J. Nilsson, Aromatic heterocycle galectin-1 interactions for selective single-digit nM affinity ligands, *RSC Adv.*, 2018, **8**(44), 24913–24922; (b) F. R. Zetterberg, K. Peterson, U. J. Nilsson, K. Andreasson Dahlgren, C. Diehl, I. Holyer, M. Hakansson, A. Khabut, B. Kahl-Knutson, H. Leffler, A. C. MacKinnon, J. A. Roper, R. J. Slack, R. Zarrizi and A. Pedersen, Discovery of the Selective and Orally Available Galectin-1 Inhibitor GB1908 as a Potential Treatment for Lung Cancer, *J. Med. Chem.*, 2024, **67**(11), 9374–9388.
- 14 T. Delaine, P. Collins, A. MacKinnon, G. Sharma, J. Stegmayr, V. K. Rajput, S. Mandal, I. Cumpstey, A. Larumbe, B. A. Salameh, B. Kahl-Knutsson, H. van Hattum, M. van Scherpenzeel, R. J. Pieters, T. Sethi, H. Schambye, S. Oredsson, H. Leffler, H. Blanchard and U. J. Nilsson, Galectin-3-Binding Glycomimetics that Strongly Reduce Bleomycin-Induced Lung Fibrosis and Modulate Intracellular Glycan Recognition, *ChemBioChem*, 2016, **17**(18), 1759–1770.
- 15 R. Paulini, K. Müller and F. Diederich, Orthogonal Multipolar Interactions in Structural Chemistry and Biology, *Angew. Chem., Int. Ed.*, 2005, **44**(12), 1788–1805.
- 16 K. Peterson, R. Kumar, O. Stenström, P. Verma, P. R. Verma, M. Håkansson, B. Kahl-Knutsson, F. Zetterberg, H. Leffler, M. Akke, D. T. Logan and U. J. Nilsson, Systematic Tuning of Fluoro-galectin-3 Interactions Provides Thiodigalactoside Derivatives with Single-Digit nM Affinity and High Selectivity, *J. Med. Chem.*, 2018, **61**(3), 1164–1175.
- 17 (a) F. R. Zetterberg, A. MacKinnon, T. Brimert, L. Gravelle, R. E. Johnsson, B. Kahl-Knutson, H. Leffler, U. J. Nilsson, A. Pedersen, K. Peterson, J. A. Roper, H. Schambye, R. J. Slack and S. Tantawi, Discovery and Optimization of the First Highly Effective and Orally Available Galectin-3 Inhibitors for Treatment of Fibrotic Disease, *J. Med. Chem.*, 2022, **65**(19), 12626–12638; (b) C. Liu, P. R. Jalagam, J. Feng, W. Wang, T. Raja, M. R. Sura, R. K. V. L. P. Manepalli, B. R. Aliphedi, S. Medavarapu, S. K. Nair, V. Muthalagu, R. Natesan, A. Gupta, B. Beno, M. Panda, K. Ghosh, J. K. Shukla, H. Sale, P. Haldar, N. Kalidindi, D. Shah, D. Patel, A. Mathur, B. A. Ellsworth, D. Cheng and A. Regueiro-Ren, Identification of Monosaccharide Derivatives as Potent, Selective, and Orally Bioavailable Inhibitors of Human and Mouse Galectin-3, *J. Med. Chem.*, 2022, **65**(16), 11084–11099; (c) F. R. Zetterberg, K. Peterson, R. E. Johnsson, T. Brimert, M. Håkansson, D. T. Logan, H. Leffler and U. J. Nilsson, Monosaccharide Derivatives with Low-Nanomolar Lectin Affinity and High Selectivity Based on Combined Fluorine-Amide, Phenyl-Arginine, Sulfur- $\pi$ , and Halogen Bond Interactions, *ChemMedChem*, 2018, **13**(2), 133–137; (d) F. R. Zetterberg, C. Diehl, M. Håkansson, B. Kahl-Knutson, H. Leffler, U. J. Nilsson, K. Peterson, J. A. Roper and R. J. Slack, Discovery of Selective and Orally Available Galectin-1 Inhibitors, *J. Med. Chem.*, 2023, **66**(24), 16980–16990.
- 18 Galecto Announces Topline Results from Phase 2b GALACTIC-1 Trial of GB0139 for the Treatment of Idiopathic Pulmonary Fibrosis. GLOBE NEWSWIRE: Boston, 2023. <https://ir.galecto.com/news-releases/news-release-details/galecto-announces-topline-results-phase-2b-galactic-1-trial/> (accessed August 2024).
- 19 (a) M. Alvala, N. S. Goud, P. S. L. Soukya, M. Ghouse, D. Komal and R. Alvala, Human galectin-1 and its inhibitors: Privileged target for cancer and HIV, *Mini-Rev. Med. Chem.*, 2019, **19**(16), 1369–1378; (b) N. S. Goud and A. Bhattacharya, Human galectin-1 in multiple cancers: A privileged molecular target in oncology, *Mini-Rev. Med. Chem.*, 2021, **21**(15), 2169–2186; (c) I. Camby, M. Le Mercier, F. Lefranc and R. Kiss, Galectin-1: a small protein with major functions, *Glycobiology*, 2006, **16**(11), 137R–157R; (d) L. S. Lau, N. B. B. Mohammed and C. J. Dimitroff, Decoding Strategies to Evade Immunoregulators Galectin-1, -3, and -9 and Their Ligands as Novel Therapeutics in Cancer Immunotherapy, *Int. J. Mol. Sci.*, 2022, **23**(24), 15554; (e) A. Sethi, S. Sanam, R. Alvala and M. Alvala, An updated patent review of galectin-1 and galectin-3 inhibitors and their potential therapeutic applications (2016–present), *Expert Opin. Ther. Pat.*, 2021, **31**(8), 709–721; (f) C. A. Orozco, N. Martinez-Bosch, P. E. Guerrero, J. Vinaixa, T. Dalotto-Moreno, M. Iglesias, M. Moreno, M. Djurec, F. Poirier, H.-J. Gabius, G. A. Rabinovich and P. Navarro, Targeting galectin-1 inhibits pancreatic cancer progression by modulating tumor-stroma crosstalk, *Proc. Natl. Acad. Sci. U. S. A.*, 2018, **115**(16), E3769–E3778; (g) L. Astorgues-Xerri, M. E. Riveiro, A. Tijeras-Raballand, M. Serova, C. Neuzillet, S. Albert, E. Raymond and S. Faivre, Unraveling galectin-1 as a novel therapeutic target for cancer, *Cancer Treat. Rev.*, 2014, **40**(2), 307–319; (h) K. Ito, K. Stannard, E. Gabutero, A. M. Clark, S.-Y. Neo, S. Onturk, H. Blanchard and S. J. Ralph, Galectin-1 as a potent target for cancer therapy: role in the tumor microenvironment, *Cancer Metastasis Rev.*, 2012, **31**(3), 763–778; (i) M. Salatino, D. O. Croci, G. A. Bianco, J. M. Ilarregui, M. A. Toscano and G. A. Rabinovich, Galectin-1 as a potential therapeutic target in autoimmune disorders and cancer, *Expert Opin. Biol. Ther.*, 2008, **8**(1), 45–57; (j) G. A. Rabinovich, Galectin-1 as a potential cancer target, *Br. J. Cancer*, 2005, **92**(7), 1188–1192; (k) C. St-Pierre, M. Ouellet, D. Giguère, R. Ohtake, R. Roy, S. Sato and M. J. Tremblay, Galectin-1-Specific Inhibitors as a New Class of Compounds To Treat HIV-1 Infection, *Antimicrob. Agents Chemother.*, 2012, **56**(1), 154–162.



- 20 (a) M. Dörr and E. Meggers, Metal complexes as structural templates for targeting proteins, *Curr. Opin. Chem. Biol.*, 2014, **19**, 76–81; (b) M. Patra and G. Gasser, The medicinal chemistry of ferrocene and its derivatives, *Nat. Rev. Chem.*, 2017, **1**(9), 0066; (c) G. Jaouen, A. Vessièrès and S. Top, Ferrocifen type anti cancer drugs, *Chem. Soc. Rev.*, 2015, **44**(24), 8802–8817.
- 21 A. Wieczorek, A. Błaż, A. Żal, H. J. Arabshahi, J. Reynisson, C. G. Hartinger, B. Rychlik and D. Plažuk, Ferrocenyl Paclitaxel and Docetaxel Derivatives: Impact of an Organometallic Moiety on the Mode of Action of Taxanes, *Chem. – Eur. J.*, 2016, **22**(32), 11413–11421.
- 22 A. Wieczorek, A. Błaż, J. Zakrzewski, B. Rychlik and D. Plažuk, Ferrocenyl 2,5-Piperazinediones as Tubulin-Binding Organometallic ABCB1 and ABCG2 Inhibitors Active against MDR Cells, *ACS Med. Chem. Lett.*, 2016, **7**(6), 612–617.
- 23 K. Schlotter, F. Boeckler, H. Hübner and P. Gmeiner, Fancy Bioisosteres: Metallocene-Derived G-Protein-Coupled Receptor Ligands with Subnanomolar Binding Affinity and Novel Selectivity Profiles, *J. Med. Chem.*, 2005, **48**(11), 3696–3699.
- 24 M. C. Martos-Maldonado, I. Quesada-Soriano, L. García-Fuentes and A. Vargas-Berenguel, Multivalent Lactose-Ferrocene Conjugates Based on Poly (Amido Amine) Dendrimers and Gold Nanoparticles as Electrochemical Probes for Sensing Galectin-3, *Nanomaterials*, 2020, **10**(2), 203.
- 25 (a) A. Dahlqvist, H. Leffler and U. J. Nilsson, C1-Galactopyranosyl Heterocycle Structure Guides Selectivity: Triazoles Prefer Galectin-1 and Oxazoles Prefer Galectin-3, *ACS Omega*, 2019, **4**(4), 7047–7053; (b) R. Roy, Y. Cao, H. Kaltner, N. Kottari, T. C. Shiao, K. Belkhadem, S. André, J. C. Manning, P. V. Murphy and H.-J. Gabius, Teaming up synthetic chemistry and histochemistry for activity screening in galectin-directed inhibitor design, *Histochem. Cell Biol.*, 2017, **147**(2), 285–301; (c) D. Giguère, S. Sato, C. St-Pierre, S. Sirois and R. Roy, Aryl O- and S-galactosides and lactosides as specific inhibitors of human galectins-1 and -3: Role of electrostatic potential at O-3, *Bioorg. Med. Chem. Lett.*, 2006, **16**(6), 1668–1672; (d) P. Sörme, Y. Qian, P.-G. Nyholm, H. Leffler and U. J. Nilsson, Low Micromolar Inhibitors of Galectin-3 Based on 3'-Derivatization of N-Acetyllactosamine, *ChemBioChem*, 2002, **3**(2–3), 183–189.
- 26 (a) B. A. Salameh, I. Cumpstey, A. Sundin, H. Leffler and U. J. Nilsson, 1H-1,2,3-Triazol-1-yl thiodigalactoside derivatives as high affinity galectin-3 inhibitors, *Bioorg. Med. Chem.*, 2010, **18**(14), 5367–5378; (b) H. Blanchard, K. Bum-Erdene and M. W. Hugo, Inhibitors of Galectins and Implications for Structure-Based Design of Galectin-Specific Therapeutics, *Aust. J. Chem.*, 2014, **67**(12), 1763–1779; (c) M. van Scherpenzeel, E. E. Moret, L. Ballell, R. M. J. Liskamp, U. J. Nilsson, H. Leffler and R. J. Pieters, Synthesis and Evaluation of New Thiodigalactoside-Based Chemical Probes to Label Galectin-3, *ChemBioChem*, 2009, **10**(10), 1724–1733; (d) H. van Hattum, H. M. Branderhorst, E. E. Moret, U. J. Nilsson, H. Leffler and R. J. Pieters, Tuning the Preference of Thiodigalactoside- and Lactosamine-Based Ligands to Galectin-3 over Galectin-1, *J. Med. Chem.*, 2013, **56**(3), 1350–1354.
- 27 M. Lamac, M. Horacek, L. C. St'astna, J. Karban, L. Sommerova, H. Skoupilova, R. Hrstka and J. Pinkas, Harmless glucose-modified ruthenium complexes suppressing cell migration of highly invasive cancer cell lines, *Appl. Organomet. Chem.*, 2020, **34**(1), e5318.
- 28 S. R. Rauthu, T. C. Shiao, S. André, M. C. Miller, É Madej, K. H. Mayo, H.-J. Gabius and R. Roy, Defining the Potential of Aglycone Modifications for Affinity/Selectivity Enhancement against Medically Relevant Lectins: Synthesis, Activity Screening, and HSQC-Based NMR Analysis, *ChemBioChem*, 2015, **16**(1), 126–139.
- 29 T. Machida, K. Lang, L. Xue, J. W. Chin and N. Winssinger, Site-Specific Glycoconjugation of Protein via Bioorthogonal Tetrazine Cycloaddition with a Genetically Encoded trans-Cyclooctene or Bicyclononyne, *Bioconjugate Chem.*, 2015, **26**(5), 802–806.
- 30 R. Šardžik, G. T. Noble, M. J. Weissenborn, A. Martin, S. J. Webb and S. L. Flitsch, Preparation of aminoethyl glycosides for glycoconjugation, *Beilstein J. Org. Chem.*, 2010, **6**, 699–703.
- 31 G. Lian, X. Zhang and B. Yu, Thioglycosides in Carbohydrate Research, *Carbohydr. Res.*, 2015, **403**, 13–22.
- 32 W. Bröder and H. Kunz, A new method of anomeric protection and activation based on the conversion of glycosyl azides into glycosyl fluorides, *Carbohydr. Res.*, 1993, **249**(1), 221–241.
- 33 J. M. Jacobson, P. I. Kitov and D. R. Bundle, The synthesis of a multivalent heterobifunctional ligand for specific interaction with Shiga toxin 2 produced by *E. coli* O157:H7, *Carbohydr. Res.*, 2013, **378**, 4–14.
- 34 M. Niemietz, L. Perkams, J. Hoffman, S. Eller and C. Unverzagt, Selective oxidative debenzoylation of mono- and oligosaccharides in the presence of azides, *Chem. Commun.*, 2011, **47**(37), 10485–10487.
- 35 O. Kanie, S. C. Crawley, M. M. Palcic and O. Hindsgaul, Acceptor-substrate recognition by N-acetylglucosaminyltransferase-V: Critical role of the 4"-hydroxyl group in  $\beta$ -D-GlcpNAc-(1  $\rightarrow$  2)- $\alpha$ -D-Manp(1  $\rightarrow$  6)- $\beta$ -D-Glcp-OR, *Carbohydr. Res.*, 1993, **243**(1), 139–164.
- 36 M. Kurfiřt, M. Dračinský, L. Červenková Šťastná, P. Cuřínová, V. Hamala, M. Hovorková, P. Bojarová and J. Karban, Selectively Deoxyfluorinated N-Acetyllactosamine Analogues as  $^{19}\text{F}$  NMR Probes to Study Carbohydrate-Galectin Interactions, *Chem. – Eur. J.*, 2021, **27**(51), 13040–13051.
- 37 J. Alais and S. David, Preparation of disaccharides having a  $\beta$ -D-mannopyranosyl group from N-phthaloyllactosamine derivatives by double or triple  $\text{S}_{\text{N}}2$  substitution, *Carbohydr. Res.*, 1990, **201**(1), 69–77.
- 38 C. Xia, W. Zhang, Y. Zhang, W. Chen, J. Nadas, R. Severin, R. Woodward, B. Wang, X. Wang, M. Kronenberg and P. G. Wang, The Roles of 3' and 4' Hydroxy Groups in



- $\alpha$ -Galactosylceramide Stimulation of Invariant Natural Killer T Cells, *ChemMedChem*, 2009, **4**(11), 1810–1815.
- 39 J. St-Gelais, V. Denavit and D. Giguere, Efficient synthesis of a galectin inhibitor clinical candidate (TD139) using a Payne rearrangement/azidation reaction cascade, *Org. Biomol. Chem.*, 2020, **18**(20), 3903–3907.
- 40 J. St-Gelais, C. Leclerc and D. Giguère, Synthesis of fluorinated thiodigalactoside analogues, *Carbohydr. Res.*, 2022, **511**, 108481.
- 41 S. Mandal and U. J. Nilsson, Tri-isopropylsilyl thioglycosides as masked glycosyl thiol nucleophiles for the synthesis of S-linked glycosides and glyco-conjugates, *Org. Biomol. Chem.*, 2014, **12**(27), 4816–4819.
- 42 X. Creary, A. Anderson, C. Brophy, F. Crowell and Z. Funk, Method for Assigning Structure of 1,2,3-Triazoles, *J. Org. Chem.*, 2012, **77**(19), 8756–8761.
- 43 D. R. van Staveren and N. Metzler-Nolte, Bioorganometallic Chemistry of Ferrocene, *Chem. Rev.*, 2004, **104**(12), 5931–5986.
- 44 J. Špaček, A. Daňhel, S. Hasoň and M. Fojta, Label-free detection of canonical DNA bases, uracil and 5-methylcytosine in DNA oligonucleotides using linear sweep voltammetry at a pyrolytic graphite electrode, *Electrochem. Commun.*, 2017, **82**, 34–38.
- 45 S. Ayaz, A. Shah and S. Munir, Investigation of Electron Transfer Mechanistic Pathways of Ferrocene Derivatives in Droplet at Carbon Electrode, *C*, 2022, **8**(3), 45.
- 46 P. Sörme, B. Kahl-Knutsson, M. Huflejt, U. J. Nilsson and H. Leffler, Fluorescence polarization as an analytical tool to evaluate galectin–ligand interactions, *Anal. Biochem.*, 2004, **334**(1), 36–47.
- 47 J. Dumić, S. Dabelić and M. Flögel, Galectin-3: An open-ended story, *Biochim. Biophys. Acta, Gen. Subj.*, 2006, **1760**(4), 616–635.
- 48 I. Cumpstey, E. Salomonsson, A. Sundin, H. Leffler and U. J. Nilsson, Double Affinity Amplification of Galectin–Ligand Interactions through Arginine–Arene Interactions: Synthetic, Thermodynamic, and Computational Studies with Aromatic Diamido Thiodigalactosides, *Chem. – Eur. J.*, 2008, **14**(14), 4233–4245.
- 49 I. Cumpstey, E. Salomonsson, A. Sundin, H. Leffler and U. J. Nilsson, Studies of Arginine–Arene Interactions through Synthesis and Evaluation of a Series of Galectin-Binding Aromatic Lactose Esters, *ChemBioChem*, 2007, **8**(12), 1389–1398.
- 50 P. Sörme, P. Arnoux, B. Kahl-Knutsson, H. Leffler, J. M. Rini and U. J. Nilsson, Structural and Thermodynamic Studies on Cation– $\pi$  Interactions in Lectin–Ligand Complexes: High-Affinity Galectin-3 Inhibitors through Fine-Tuning of an Arginine–Arene Interaction, *J. Am. Chem. Soc.*, 2005, **127**(6), 1737–1743.
- 51 (a) P. Sindrewicz, X. Li, E. A. Yates, J. E. Turnbull, L.-Y. Lian and L.-G. Yu, Intrinsic tryptophan fluorescence spectroscopy reliably determines galectin-ligand interactions, *Sci. Rep.*, 2019, **9**(1), 11851; (b) A. Göhler, C. Büchner, S. André, S. Doose, H. Kaltner and H. J. Gabius, Sensing ligand binding to a clinically relevant lectin by tryptophan fluorescence anisotropy, *Analyst*, 2011, **136**(24), 5270–5276.
- 52 (a) E. Paleček, J. Tkáč, M. Bartošík, T. Bertók, V. Ostatná and J. Paleček, Electrochemistry of Nonconjugated Proteins and Glycoproteins. Toward Sensors for Biomedicine and Glycomics, *Chem. Rev.*, 2015, **115**(5), 2045–2108; (b) H. Černocká, P. Vonka, V. Kasalová, L. Sommerova, V. Vandova, R. Hrstka and V. Ostatná, AGR2-AGR3 hetero-oligomeric complexes: Identification and characterization, *Bioelectrochemistry*, 2021, **140**, 107808.
- 53 V. Ostatná, V. Kasalová-Vargová, L. Kékedy-Nagy, H. Černocká and E. E. Ferapontova, Chronopotentiometric sensing of specific interactions between lysozyme and the DNA aptamer, *Bioelectrochemistry*, 2017, **114**, 42–47.
- 54 V. Vargová, R. Helma, E. Paleček and V. Ostatná, Electrochemical sensing of concanavalin A and ovalbumin interaction in solution, *Anal. Chim. Acta*, 2016, **935**, 97–103.
- 55 K. J. Bowers, D. E. Chow, H. Xu, R. O. Dror, M. P. Eastwood, B. A. Gregersen, J. L. Klepeis, I. Kolossvary, M. A. Moraes, F. D. Sacerdoti, J. K. Salmon, Y. Shan and D. E. Shaw, In Scalable Algorithms for Molecular Dynamics Simulations on Commodity Clusters, SC '06: Proceedings of the 2006 ACM/IEEE Conference on Supercomputing, 11–17 Nov. 2006; 2006; pp 43–43.
- 56 *Schrödinger Release 2024-1*, Desmond Molecular Dynamics System, Schrödinger, Inc, New York, 2024.
- 57 J. J. P. Stewart, *MOPAC2016*, Stewart Computational Chemistry: Colorado Springs, CO, USA, 2016.
- 58 (a) C. Atmanene, C. Ronin, S. Téletchéa, F.-M. Gautier, F. Djedaïni-Pilard, F. Ciesielski, V. Vivat and C. Grandjean, Biophysical and structural characterization of mono/di-arylated lactosamine derivatives interaction with human galectin-3, *Biochem. Biophys. Res. Commun.*, 2017, **489**(3), 281–286; (b) J. Seetharaman, A. Kanigsberg, R. Slaaby, H. Leffler, S. H. Barondes and J. M. Rini, X-ray Crystal Structure of the Human Galectin-3 Carbohydrate Recognition Domain at 2.1 Å Resolution\*, *J. Biol. Chem.*, 1998, **273**(21), 13047–13052; (c) A. Gimeno, S. Delgado, P. Valverde, S. Bertuzzi, M. A. Berbís, J. Echavarren, A. Lacetera, S. Martín-Santamaría, A. Surolia, F. J. Cañada, J. Jiménez-Barbero and A. Ardá, Minimizing the Entropy Penalty for Ligand Binding: Lessons from the Molecular Recognition of the Histo Blood-Group Antigens by Human Galectin-3, *Angew. Chem., Int. Ed.*, 2019, **58**(22), 7268–7272; (d) S. Bertuzzi, A. Gimeno, R. Núñez-Franco, G. Bernardo-Seisdedos, S. Delgado, G. Jiménez-Osés, O. Millet, J. Jiménez-Barbero and A. Ardá, Unravelling the Time Scale of Conformational Plasticity and Allostery in Glycan Recognition by Human Galectin-1, *Chem. – Eur. J.*, 2020, **26**(67), 15643–15653.
- 59 R. Wang, H. Chen, W. Yan, M. Zheng, T. Zhang and Y. Zhang, Ferrocene-containing hybrids as potential anti-cancer agents: Current developments, mechanisms of action and structure-activity relationships, *Eur. J. Med. Chem.*, 2020, **190**, 112109.



- 60 B. Sharma and V. Kumar, Has Ferrocene Really Delivered Its Role in Accentuating the Bioactivity of Organic Scaffolds?, *J. Med. Chem.*, 2021, **64**(23), 16865–16921.
- 61 (a) A. Hottin, F. Dubar, A. Steenackers, P. Delannoy, C. Biot and J.-B. Behr, Iminosugar–ferrocene conjugates as potential anticancer agents, *Org. Biomol. Chem.*, 2012, **10**(29), 5592–5597; (b) T. Hodik, M. Lamac, L. C. Stastna, J. Karban, L. Koubkova, R. Hrstka, I. Cisarova and J. Pinkas, Titanocene Dihalides and Ferrocenes Bearing a Pendant  $\alpha$ -D-Xylofuranos-5-yl or  $\alpha$ -D-Ribofuranos-5-yl Moiety. Synthesis, Characterization, and Cytotoxic Activity, *Organometallics*, 2014, **33**(8), 2059–2070; (c) T. Hodik, M. Lamac, L. C. Stastna, P. Curinova, J. Karban, H. Skoupilova, R. Hrstka, I. Cisarova, R. Gyepes and J. Pinkas, Improving cytotoxic properties of ferrocenes by incorporation of saturated N-heterocycles, *J. Organomet. Chem.*, 2017, **846**, 141–151; (d) R. Trivedi, S. B. Deepthi, L. Giribabu, B. Sridhar, P. Sujitha, C. Ganesh Kumar and K. V. S. Ramakrishna, Synthesis, crystal structure, electronic spectroscopy, electrochemistry and biological studies of carbohydrate containing ferrocene amides, *Appl. Organomet. Chem.*, 2012, **26**(7), 369–376.

